On algebraic damping close to inhomogeneous Vlasov equilibria in multi-dimensional spaces

Julien Barre, Yoshiyuki Yamaguchi

On algebraic damping close to inhomogeneous Vlasov equilibria in multi-dimensional spaces

Julien Barré[1] **and Yoshiyuki Y Yamaguchi**[2]

[1] Laboratoire J.A. Dieudonné, Université de Nice Sophia-Antipolis, UMR CNRS 7351, Parc Valrose, F-06108 Nice Cedex 02, France

[2] Department of Applied Mathematics and Physics, Graduate School of Informatics, Kyoto University, Kyoto 606-8501, Japan

E-mail: jbarre@unice.fr

Abstract. We investigate the asymptotic damping of a perturbation around inhomogeneous stable stationary states of the Vlasov equation in spatially multi-dimensional systems. We show that branch singularities of the Fourier-Laplace transform of the perturbation yield algebraic dampings. In two spatial dimensions, we classify the singularities and compute the associated damping rate and frequency. This 2D setting also applies to spherically symmetric self-gravitating systems. We validate the theory using a toy model and an advection equation associated with the isochrone model, a model of spherical self-gravitating systems.

PACS numbers: 05.20.Dd, 45.50.-j, 52.25.Dg, 98.10.+z

Submitted to: *J. Phys. A: Math. Gen.*

1. Introduction

The Vlasov equation, often called Collisionless Boltzmann equation, describes, over a certain time frame, the large scale dynamics of Hamiltonian systems of interacting particles, in the limit where each particle feels the effect of many others. It is thus found in many fields, among which plasma physics of course, and astrophysics, where it describes self-gravitating systems.

The Vlasov equation shows a notoriously rich dynamics. First, it possesses a continuous infinity of stationary states, whose study may in itself be a complicated problem. The next problem, the study of the linearized dynamics close to a stationary state, has a long story. In 1946, Landau [1] formally showed that close to a stable homogeneous stationary state, a density perturbation may decay exponentially, which was a very surprising result for a Hamiltonian system. This was the starting point of an extremely abundant physical literature. On the mathematical side, it has been proved that Landau analysis is correct [2, 3]. It is also known that the exponential damping fails when the reference state or the perturbation is not analytic [4], or the spatial domain unbounded [5].

The non-linear case, that is the study of a perturbation close to a homogeneous stationary state, under the full Vlasov dynamics, is much more complicated. The subject has witnessed spectacular progresses recently [6, 7, 8].

Most studies on Landau damping deal with homogeneous stationary states. By comparison, the literature on perturbations of inhomogeneous states is less developed, although these states are very important. Despite the technical difficulties involved, a lot of work has been done in the astrophysical literature. Kalnajs [9], and then Polyachenko and Schuckman [10] have developed a powerful formalism, sometimes called the "matrix method", to solve the linearized Vlasov equation in a inhomogeneous context. Since then, it has been used to study the instability of many models of stellar systems, and compute the growth rates (see [11] for a textbook account). Some other methods to compute instability rates have been introduced and applied to toy models recently [12, 13, 14]. Purely oscillating modes in 1D have been investigated in [15]. Also, when the question is to prove stability and not to compute a decay rate, there exist powerful variational methods [11]. However, computing decay rates for non-oscillating stable situations is more tricky than computing instability rates, since it involves an additional analytic continuation, as in Landau's original analysis. In the astrophysical literature, we are aware of only two papers performing this continuation numerically, and thus explicitly computing the analog of Landau damping rates [16, 17]. In [18], the continuation is performed analytically, but on a one dimensional toy model. Thus, although Landau damping is considered an important player in the dynamics of stellar systems (see for instance [11]), there are very few actual computations of damping rates close to inhomogeneous stationary states.

In addition, these studies done in the astrophysical context do not mention a fundamental difference between homogeneous and inhomogeneous stationary states: in

the inhomogeneous case, no matter what is the regularity of the stationary state and the perturbation, the asymptotic linear decay is never exponential. This has been seen in the Kuramoto model, which shares some properties with the Vlasov equation [19], and on a type of Vlasov equation in [20]. The picture is as follows: the dynamics may show a transient exponential decay governed by a Landau pole, but the asymptotic decay is always algebraic. This phenomenology is also well known for the 2D Euler equation [21], which is in many respects similar to the Vlasov equation. We note that such algebraic decays may also arise close to a homogeneous state, when the perturbation or the reference state is not regular enough [4]; we stress that the situation is different close to inhomogeneous states, because the algebraic decay occurs for all reference states and perturbations. [22] contains a detailed analysis of this phenomenon in 1D, including derivation of the decay exponents and comparison with direct numerical simulations. In this paper, we extend the analysis of [22] to multidimensional systems, putting our emphasis on 2D systems and 3D systems with spherical symmetry. These includes some important models of stellar systems.

More specifically, we first use the standard matrix method to formally solve the linear dynamics in a Laplace transformed space (section 2). From this starting point:
i) we identify and classify the singularities appearing in the Laplace transform of the perturbation. It turns out that the zoology of singularities in two dimensions is much richer than in one dimension, see section 3.
ii) we exhibit the asymptotic decay for each type of singularities in section 4.
iii) we introduce advection equations associated with the linearized Vlasov equations in section 5. These advection equations have a solution in integral form; hence the numerical task to obtain the temporal evolution of the system is reduced from solving the (linearized) Vlasov equation in $2d$-dimensional phase space to performing integrals in a d-dimensional space, where d is the spatial dimension.
iv) Using the above theory, we analyze the asymptotic decay of a perturbation in a toy model and a spherically symmetric stellar model, and check the theory against the numerically computed exact solutions to the simple advection models, see sections 6.4, 7.

Our analysis of the asymptotic decay of a perturbation is formal, and moreover relies on the linearized Vlasov equation. There is no guarantee that this is relevant to understand the asymptotic decay of the non-linear Vlasov equation. In principle, our results should then be supplemented by direct numerical simulations of the full Vlasov equation. However, such simulations are difficult in more than one spatial dimension, since we are aiming at an asymptotic in time regime, while keeping a good spatial precision. We left this study for future work. This is why we analyze instead with the present theory easily solvable linear advection equations, for illustrative purpose.

2. Solution to the linearized Vlasov equation: the matrix method

Throughout the paper, we will use bold letters ($\boldsymbol{q}$, $\boldsymbol{p}$, $\boldsymbol{\theta}$, $\boldsymbol{J}$, ...) to denote vectors.

2.1. System

We start with the Vlasov equation in d spatial dimensions for the one-particle distribution function $f(\boldsymbol{q}, \boldsymbol{p}, t)$,

$$\partial_t f + \nabla_{\boldsymbol{p}} H \cdot \nabla_{\boldsymbol{q}} f - \nabla_{\boldsymbol{q}} H \cdot \nabla_{\boldsymbol{p}} f = 0, \tag{1}$$

where $\boldsymbol{q} \in X \subset \mathbb{R}^d$ is the position variable, $\boldsymbol{p} \in \mathbb{R}^d$ the conjugate momentum variable, and $\nabla_{\boldsymbol{q}}$, $\nabla_{\boldsymbol{p}}$ denote respectively the gradients with respect to $\boldsymbol{q}$ and $\boldsymbol{p}$. The domain X is $\mathbb{R}^3$ in a stellar system, and $[0, 2\pi)^d$ if the system has periodic boundary conditions. H is the one-particle Hamiltonian defined by

$$H[f](\boldsymbol{q}, \boldsymbol{p}, t) = \frac{\boldsymbol{p}^2}{2} + \Phi[f](\boldsymbol{q}, t) + \Phi_{\text{ext}}(\boldsymbol{q}). \tag{2}$$

The potential $\Phi[f](\boldsymbol{q}, t)$ is defined from the two-body interaction potential v and the distribution f as

$$\Phi[f](\boldsymbol{q}, t) = \int_{\mathbb{R}^d} d\boldsymbol{p} \int_X d\boldsymbol{q}\ v(\boldsymbol{q} - \boldsymbol{q}') f(\boldsymbol{q}', \boldsymbol{p}, t). \tag{3}$$

The external potential $\Phi_{\text{ext}}(\boldsymbol{q})$ creates a force $F_{\text{ext}}(\boldsymbol{q})$:

$$F_{\text{ext}}(\boldsymbol{q}) = -\nabla_{\boldsymbol{q}} \Phi_{\text{ext}}(\boldsymbol{q}). \tag{4}$$

Let f_0 be a stationary solution to the Vlasov equation (1). For the stationary solution, the potential $\Phi[f_0]$ and the one-particle Hamiltonian $H[f_0]$ are independent of time. In this paper, we limit ourselves to situations where the one-particle Hamiltonian $H[f_0]$ is integrable. Thus, we may introduce actions $\boldsymbol{J} = (J_1, \ldots, J_d)$ and conjugate angles $\boldsymbol{\theta} = (\theta_1, \ldots, \theta_d)$, and the one-particle Hamiltonian is a function of the actions only, i.e. $H[f_0](\boldsymbol{J})$. A practically important example is given by spherically symmetric stellar systems, see section 3.1. A stationary solution can be constructed by taking f_0 as a function of actions, satisfying self-consistent conditions, since the actions depend on f_0 through the potential $\Phi[f_0]$.

We now consider a small perturbation to a stationary solution $f_0(\boldsymbol{J})$:

$$f(\boldsymbol{\theta}, \boldsymbol{J}, t) = f_0(\boldsymbol{J}) + f_1(\boldsymbol{\theta}, \boldsymbol{J}, t) \tag{5}$$

and write the linearized Vlasov equation for f_1:

$$\partial_t f_1 + \boldsymbol{\Omega}(\boldsymbol{J}) \cdot \nabla_{\boldsymbol{\theta}} f_1 - \nabla_{\boldsymbol{J}} f_0 \cdot \nabla_{\boldsymbol{\theta}} \Phi_1 = 0\ , \tag{6}$$

where $\Phi_1 = \Phi[f_1]$ is the perturbed potential

$$\Phi_1(\boldsymbol{q}, t) = \int_{\mathbb{R}^d} \int_X v(\boldsymbol{q} - \boldsymbol{q}') f_1(\boldsymbol{q}', \boldsymbol{p}, t) d\boldsymbol{q}' d\boldsymbol{p}, \tag{7}$$

and $\boldsymbol{\Omega}(\boldsymbol{J}) = \nabla_{\boldsymbol{J}} H[f_0](\boldsymbol{J})$ is the vector of the frequencies in the unperturbed potential.

2.2. Fourier-Laplace transform

To analyze the linearized Vlasov equation (6), we introduce the Fourier-Laplace transform $\hat{u}(\boldsymbol{m}, \boldsymbol{J}, \omega)$ of a function $u(\boldsymbol{\theta}, \boldsymbol{J}, t)$ as

$$\hat{u}(\boldsymbol{m}, \boldsymbol{J}, \omega) = \int_{-\pi}^{\pi} d\boldsymbol{\theta}\ e^{-i\boldsymbol{m}\cdot\boldsymbol{\theta}} \int_0^{+\infty} dt\ e^{i\omega t} u(\boldsymbol{\theta}, \boldsymbol{J}, t) \tag{8}$$

where $\boldsymbol{m} = (m_1, \ldots, m_d)$ is a d-uplet of integers, $\boldsymbol{m}\cdot\boldsymbol{\theta}$ is the Euclidian inner product and $\mathrm{Im}(\omega)$ is large enough to ensure convergence of the integral with respect to t. The inverse transform is then

$$u(\boldsymbol{\theta}, \boldsymbol{J}, t) = \frac{1}{(2\pi)^{d+1}} \sum_{\boldsymbol{m}\in\mathbb{Z}^d} e^{i\boldsymbol{m}\cdot\boldsymbol{\theta}} \int_\Gamma d\omega\ e^{-i\omega t}\ \hat{u}(\boldsymbol{m}, \boldsymbol{J}, \omega) \tag{9}$$

where Γ is a Bromwich contour running from $-\infty + i\sigma$ to $+\infty + i\sigma$, and the real value σ is larger than the imaginary part of any singularity of $\hat{u}(\boldsymbol{m}, \boldsymbol{J}, \omega)$ in the complex ω-plane.

Simple and standard algebraic manipulations on (6) yield the following expression for the Fourier-Laplace transform of the perturbation:

$$\hat{f}_1(\boldsymbol{m}, \boldsymbol{J}, \omega) = A(\boldsymbol{m}, \boldsymbol{J}, \omega)\hat{\Phi}_1(\boldsymbol{m}, \boldsymbol{J}, \omega) + B(\boldsymbol{m}, \boldsymbol{J}, \omega), \tag{10}$$

where

$$A(\boldsymbol{m}, \boldsymbol{J}, \omega) = \frac{\boldsymbol{m}\cdot\nabla_{\boldsymbol{J}} f_0(\boldsymbol{J})}{\boldsymbol{m}\cdot\boldsymbol{\Omega}(\boldsymbol{J}) - \omega}, \tag{11}$$

$$B(\boldsymbol{m}, \boldsymbol{J}, \omega) = \frac{g(\boldsymbol{m}, \boldsymbol{J})}{\boldsymbol{m}\cdot\boldsymbol{\Omega}(\boldsymbol{J}) - \omega}, \tag{12}$$

and $ig(\boldsymbol{m}, \boldsymbol{J})$ is the Fourier transform of the initial perturbation $f_1(\boldsymbol{\theta}, \boldsymbol{J}, t = 0)$ with respect to $\boldsymbol{\theta}$. Without loss of generality, we assume

$$g(\boldsymbol{0}, \boldsymbol{J}) = 0. \tag{13}$$

Notice that we can always include a non-zero $g(\boldsymbol{0}, \boldsymbol{J})$ in the stationary state f_0.

2.3. Biorthogonal functions

We should now solve the two coupled equations (7) and (10) to find f_1 and Φ_1. The usual strategy at this point is to introduce two families of biorthogonal functions [9, 10, 23]. The computations below are standard (for a textbook reference, see for instance [11]); we reproduce them here to ensure that this article is self-contained.

We expand any density function $\rho(\boldsymbol{q})$ on the basis $\{d_i(\boldsymbol{q})\}_{i\in I}$:

$$\rho(\boldsymbol{q}) = \sum_{i\in I} a_i d_i(\boldsymbol{q}) \tag{14}$$

and any potential function $\Phi(\boldsymbol{q})$ on the basis $\{u_k(\boldsymbol{q})\}_{k\in K}$:

$$\Phi(\boldsymbol{q}) = \sum_{k\in K} b_k u_k(\boldsymbol{q}). \tag{15}$$

The two index sets I and K satisfy $K \subset I \subset \mathbb{Z}$, and the two basis $\{d_i\}_{i\in I}$ and $\{u_k\}_{k\in K}$ are chosen such that

(i) the two families are orthogonal to each other:

$$(d_i, u_k) = \int_{\mathbb{R}^d} d_i(\boldsymbol{q})\bar{u}_k(\boldsymbol{q})d\boldsymbol{q} = \lambda_k \delta_{ik}, \quad (i \in I,\ k \in K) \tag{16}$$

with $\lambda_k \neq 0$, and where δ_{ik} is the Kronecker δ.

(ii) u_k is the potential created by the density distribution d_i:

$$\int_{\mathbb{R}^d} v(\boldsymbol{q}-\boldsymbol{q}')d_i(\boldsymbol{q}')d\boldsymbol{q}' = \begin{cases} u_i(\boldsymbol{q}) & (i \in K) \\ 0 & (i \notin K) \end{cases} \tag{17}$$

Assuming we have at hand two such families of biorthogonal functions, we expand the perturbation density

$$\rho_1(\boldsymbol{q}, t) = \int_{\mathbb{R}^d} f_1(\boldsymbol{q}, \boldsymbol{p}, t)d\boldsymbol{p} \tag{18}$$

and potential as

$$\rho_1(\boldsymbol{q}, t) = \sum_{i \in I} a_i(t)d_i(\boldsymbol{q}) \tag{19}$$

$$\Phi_1(\boldsymbol{q}, t) = \sum_{k \in K} a_k(t)u_k(\boldsymbol{q}). \tag{20}$$

Properties (16) and (17) ensure that the coefficients are identical for ρ_1 and Φ_1.

Using (20), we first compute $\hat{\Phi}_1$, the Fourier-Laplace transform of Φ_1:

$$\hat{\Phi}_1(\boldsymbol{m}, \boldsymbol{J}, \omega) = \sum_{k \in K} \tilde{a}_k(\omega)c_k(\boldsymbol{m}, \boldsymbol{J}) \tag{21}$$

where $\tilde{a}_k$ is the Laplace transform of a_k, and $c_k(\boldsymbol{m}, \boldsymbol{J})$ is the Fourier transform of u_k:

$$c_k(\boldsymbol{m}, \boldsymbol{J}) = \int u_k(\boldsymbol{q})e^{-i\boldsymbol{m}\cdot\boldsymbol{\theta}}d\boldsymbol{\theta}. \tag{22}$$

Substituting (21) into (10), and performing the inverse Fourier transform, we obtain an expression for $\tilde{f}_1(\boldsymbol{\theta}, \boldsymbol{J}, \omega)$, the Laplace transform of the perturbation:

$$\tilde{f}_1 = \frac{1}{(2\pi)^d} \sum_{\boldsymbol{m} \in \mathbb{Z}^d} \left(\frac{\boldsymbol{m} \cdot \nabla_{\boldsymbol{J}} f_0}{\boldsymbol{m} \cdot \boldsymbol{\Omega} - \omega} \sum_{k \in K} \tilde{a}_k(\omega)c_k(\boldsymbol{m}, \boldsymbol{J}) + \frac{g(\boldsymbol{m}, \boldsymbol{J})}{\boldsymbol{m} \cdot \boldsymbol{\Omega} - \omega} \right) e^{i\boldsymbol{m}\cdot\theta}. \tag{23}$$

Now, we multiply (23) by $\bar{u}_l(\boldsymbol{q})$ $(l \in K)$ and integrate over $d\boldsymbol{\theta}d\boldsymbol{J}$. We compute the left hand side using the change of variables $(\boldsymbol{\theta}, \boldsymbol{J}) \to (\boldsymbol{q}, \boldsymbol{p})$ which has Jacobian 1, and the property (16): the result is $\lambda_l \tilde{a}_l(\omega)$. In the right hand side, performing the integration over $\boldsymbol{\theta}$ introduces the functions $\bar{c}_l(\boldsymbol{m}, \boldsymbol{J})$. The result is

$$\lambda_l \tilde{a}_l(\omega) = \sum_{k \in K} F_{lk}(\omega)\tilde{a}_k(\omega) + G_l(\omega) \tag{24}$$

with

$$F_{lk}(\omega) = \frac{1}{(2\pi)^d} \sum_{\boldsymbol{m} \in \mathbb{Z}^d} \int \frac{\boldsymbol{m} \cdot \nabla_{\boldsymbol{J}} f_0(\boldsymbol{J})}{\boldsymbol{m} \cdot \boldsymbol{\Omega}(J) - \omega} \bar{c}_l(\boldsymbol{m}, \boldsymbol{J})c_k(\boldsymbol{m}, \boldsymbol{J})d\boldsymbol{J} \quad (l, k \in K) \tag{25}$$

and

$$G_l(\omega) = \frac{1}{(2\pi)^d} \sum_{\boldsymbol{m} \in \mathbb{Z}^d} \int \frac{g(\boldsymbol{m}, \boldsymbol{J})}{\boldsymbol{m} \cdot \boldsymbol{\Omega}(J) - \omega} \bar{c}_l(\boldsymbol{m}, \boldsymbol{J})d\boldsymbol{J} \quad (l \in K). \tag{26}$$

The contributions from $\boldsymbol{m} = \boldsymbol{0}$ clearly vanish for F_{lk}, and also for G_l, thanks to assumption (13). Defining the $(\sharp K) \times (\sharp K)$ matrices Λ and $F(\omega) = (F_{lk}(\omega))$, where Λ is diagonal with elements $\{\lambda_l\}_{l\in K}$, and the $(\sharp K)$-dimensional vectors $G(\omega) = (G_l(\omega))$ and $\tilde{a}(\omega) = (\tilde{a}_k(\omega))$, the above equations may be rewritten in compact form:

$$[\Lambda - F(\omega)]\tilde{a}(\omega) = G(\omega). \tag{27}$$

The formal solution for $\tilde{a}$ is

$$\tilde{a}(\omega) = [\Lambda - F(\omega)]^{-1} G(\omega). \tag{28}$$

The equation $\det(\Lambda - F(\omega)) = 0$ is sometimes called the dispersion relation.

2.4. Analytic continuation

Assuming that the decay for large $\boldsymbol{J}$ is fast enough in the integrands, and that the $c_k(\boldsymbol{m}, \boldsymbol{J})$ are regular, expressions (25) and (26) show that functions $F_{lk}(\omega)$ and $G_k(\omega)$ are analytic in the upper half plane $\mathrm{Im}(\omega) > 0$, since the corresponding integrals over $\boldsymbol{J}$ have no singularity. The integrands are singular however for any real ω at which $\boldsymbol{m}\cdot\boldsymbol{\Omega}(\boldsymbol{J}) - \omega$ vanishes. Thus, expressions (25) and (26) should be analytically continued to define the F's, G's and $\tilde{a}$'s in the lower half plane $\mathrm{Im}(\omega) \leq 0$. This analytical continuation is a generalization of the usual Landau prescription in 1D. It is sketched in some details in the 2D case in section 3.2.

The last step to compute the evolution of the perturbation is to perform an inverse Laplace transform on the functions $\tilde{a}(\omega)$. The large time behaviour of $a_k(t)$ is determined by the singularities of $\tilde{a}_k(\omega)$: our goal now is then to study and classify the singularities of $\tilde{a}(\omega)$.

2.5. Singularities of $\tilde{a}(\omega)$ and roots of the dispersion relation

The singularities of $\tilde{a}$ may come (i) from the roots of the dispersion relation $\det(\Lambda - F(\omega)) = 0$, and (ii) from singularities of the functions F's and G's themselves. We discuss the former singularities in this section: we will see that these singularities do not dominate in the asymptotic regime. The dominating latter singularities are classified in the next section in the two-dimensional setting.

Roots of the dispersion relation $\det(\Lambda - F(\omega)) = 0$ yield poles for the functions $\tilde{a}_j$. Such poles in the upper half plane correspond to eigenvalues of the linearized Vlasov operator, with exponentially growing eigenmodes. Since we are interested in the relaxation of a perturbation close to a stable stationary state of the Vlasov equation, we assume that there are no such eigenmodes. Poles on the real axis correspond to purely oscillating eigenmodes. In order to study the decay of perturbations, we also assume that there are no such modes. There may be roots of the dispersion relation in the lower half plane $\mathrm{Im}(\omega) < 0$ (in this case, they are rather roots of the analytic continuation of the dispersion relation). These are the usual "Landau poles", giving rise to exponential damping. This damping may be an important feature of the dynamics at intermediate

time scales, especially if the pole is close to the real axis [16, 17, 18], but the asymptotic regime is always dominated by the singularities of the functions F's and G's, as will become clear in the following sections.

3. Singularities of F and G in two-dimensional setting

We have seen that the functions F's and G's have no singularities for $\mathrm{Im}(\omega) > 0$. The integrands of F's and G's are singular for $\boldsymbol{J}$'s such that $\boldsymbol{m} \cdot \boldsymbol{\Omega}(\boldsymbol{J}) - \omega$ vanishes, and these singularities may yield branch points on the real ω axis. Thus, to investigate the asymptotic behaviour of a perturbation due to these branch points, we turn now to the singularities on the real axis. From now on and for simplicity, we restrict ourselves to two-dimensional integrations over $\boldsymbol{J} = (J_1, J_2)$ in the formulas (25) and (26) entering into the definitions of F and G. We have in mind perturbations in spherically symmetric self-gravitating systems, which fit into this two-dimensional setting, as shown in section 3.1. There would be no major obstacles to an analysis in higher dimension, except the growing number and complexity of the possible types of singularities.

3.1. Spherically symmetric system

Although Vlasov-type equations appear in various settings, the main situation we have in mind is the dynamics of a perturbation of a spherical self-gravitating system. The dynamics in the potential created by the stationary distribution is then integrable. It is customary [11] to use as actions J_r ("radial action"), L (modulus of the angular momentum) and L_z (projection on the z axis of the angular momentum). The radial action J_r, energy E of a particle and angular momentum L are related by

$$J_r = \frac{1}{\pi} \int_{r_{min}}^{r_{max}} \sqrt{2E - 2\Phi(r) - \frac{L^2}{r^2}} dr \tag{29}$$

where $\Phi(r)$ is the potential created by the stationary state and r_{min} and r_{max} are the minimum and maximum distance from the origin reached by the particle. In this coordinate system, the one-particle Hamiltonian depends only on the actions J_r and L.

Let us assume that f_0 and g depend on the actions only through the one-particle Hamiltonian. Then, $f_0(\boldsymbol{J})$, $g(\boldsymbol{J})$ and $c_k(\boldsymbol{m}, \boldsymbol{J})$ depend only on actions J_r and L, and hence the potentially singular integrands in (25) and (26) also depend only on J_r and L. The three-dimensional integrals are thus reduced to two-dimensional integrals. The case of spherically symmetric systems is then included in the abstract setting introduced in section 3.2.

3.2. An abstract problem

The abstract problem is to study the singularities of the analytic continuation of $\varphi(z)$ defined for $\mathrm{Im}(z) > 0$ as integrals over a domain $D \subset \mathbb{R}^2$:

$$\varphi(z) = \int_{D\subset\mathbb{R}^2} \frac{\nu(\boldsymbol{J})}{\mu(\boldsymbol{J}) - z} d\boldsymbol{J} \tag{30}$$

with μ and ν real functions. Functions F and G, (25) and (26) respectively, fit in this framework, with $\mu(\boldsymbol{J}) = \boldsymbol{m} \cdot \boldsymbol{\Omega}(\boldsymbol{J})$, and by defining properly $\nu(\boldsymbol{J})$. We assume $\boldsymbol{m} \neq \boldsymbol{0}$ since the contributions from $\boldsymbol{m} = \boldsymbol{0}$ in the definitions of F and G vanish. We also assume that μ and ν are very regular: although they are naturally defined over the domain $D \subset \mathbb{R}^2$, they may be analytically continued over the complex $\boldsymbol{J}$ domain. We further assume that their integrability properties are as good as needed. Our goal is to study the singularities of the function

$$\phi(x) = \lim_{y\to 0^+} \varphi(x + iy), \text{ with } x, y \in \mathbb{R}. \tag{31}$$

This is the analytic continuation on the real axis of $\varphi(z)$, which is a priori defined for $\mathrm{Im}(z) > 0$.

For z real, the denominator in (30), $\mu(\boldsymbol{J}) - z$, may vanish. We explain in Appendix A why for a generic z there exists an analytic continuation of φ in a neighborhood of z, and hence there is no singularity for ϕ. From the computation in Appendix A, special values of $x_0 = \mu(\boldsymbol{J}^*)$ corresponding to a singularity for ϕ are easily identified; we classify the special points $\boldsymbol{J}^*$ and the associated singularities for ϕ in the following subsections:

(i) Vertex singularity: a point $\boldsymbol{J}^*$ at which the boundary of D is not regular (section 3.3)

(ii) Tangent singularity: a point $\boldsymbol{J}^*$ at which the level set $\mu(\boldsymbol{J}) = \mu(\boldsymbol{J}^*)$ is tangent to the boundary of D (section 3.4).

(iii) Critical singularity: a critical point $\boldsymbol{J}^*$ of the function $\mu(\boldsymbol{J})$ inside D (section 3.5).

We will compute singularities of $\phi(x)$ around $x_0 = \mu(\boldsymbol{J}^*)$ by expanding $\mu(\boldsymbol{J})$ around $\boldsymbol{J}^*$:

$$\begin{aligned}\mu(\boldsymbol{J}) = x_0 &+ \mu_1(J_1 - J_1^*) + \mu_2(J_2 - J_2^*) + \frac{1}{2}\mu_{11}(J_1 - J_1^*)^2 \\ &+ \frac{1}{2}\mu_{22}(J_2 - J_2^*)^2 + \mu_{12}(J_1 - J_1^*)(J_2 - J_2^*) + \cdots\end{aligned} \tag{32}$$

where, for instance, μ_i $(i = 1, 2)$ represents $(\partial\mu/\partial J_i)(\boldsymbol{J}^*)$ and is not zero in general. The above three types of singularities (i), (ii) and (iii) appear at the point $\boldsymbol{J}^*$ where respectively (i) neither μ_1 nor μ_2 vanish, (ii) μ_1 or μ_2 vanishes, but not both, and (iii) both μ_1 and μ_2 vanish. The three types of singularities have therefore respectively 0, 1 and 2 analytic conditions for $\mu(\boldsymbol{J})$, and 2, 1 and 0 geometric conditions; see Table 1. Considering that there are two variables J_1 and J_2, these singularities appear generically. Special treatments are devoted to the case of an infinite domain D (section 3.6), and to a special situation which however does arise generically for spherically symmetric self-gravitating systems (section 3.7).

Singularity	**Conditions for $\mu(\boldsymbol{J})$**	**Geometric conditions at $\boldsymbol{J}^*$**
Vertex	—	On ∂D, non-regular point
Tangent	$\mu_1 = 0$ or $\mu_2 = 0$	On ∂D
Critical	$\mu_1 = 0$ and $\mu_2 = 0$	—

Table 1. Summary for the vertex, tangent and critical singularities. μ_i represents $(\partial\mu/\partial J_i)(\boldsymbol{J}^*)$ for $i = 1, 2$, and is not zero in general. The symbol ∂D denotes the boundary of D. The "or" in tangent singularity is exclusive.

3.3. Vertex singularity

We consider first a singular point $\boldsymbol{J}^*$ on the boundary of the domain D, such that there is a jump in the boundary's slope at $\boldsymbol{J}^*$. We refer to such a point as a "vertex", see figure 1. This type of singularity is always present in spherical self-gravitating systems at zero radial action and zero angular momentum.

To investigate the leading singularity of $\phi(x)$ created by the vertex, it is enough to keep only the leading order terms in the expansions of $\mu(\boldsymbol{J})$ and $\nu(\boldsymbol{J})$. We expand the function $\mu(\boldsymbol{J})$ as

$$\mu(\boldsymbol{J}) \simeq x_0 + \mu_1(J_1 - J_1^*) + \mu_2(J_2 - J_2^*) \tag{33}$$

where $x_0 = \mu(\boldsymbol{J}^*)$, and $\nu(\boldsymbol{J})$ as

$$\nu(\boldsymbol{J}) \sim C(J_1 - J_1^*)^{a_1}(J_2 - J_2^*)^{a_2}, \tag{34}$$

where a_1 and a_2 are non-negative integers. We assume that the first-order derivatives μ_1 and μ_2 do not vanish, which should be the generic case. Here and in the following C is a constant whose value plays no role and may vary from line to line.

The singularity of $\phi(x)$ is then investigated on the following reduced expression for $\varphi(z)$

$$\varphi(z) = C \int_{U_{\boldsymbol{J}^*}} \frac{(J_1 - J_1^*)^{a_1}(J_2 - J_2^*)^{a_2}}{\mu_1(J_1 - J_1^*) + \mu_2(J_2 - J_2^*) - (z - x_0)} dJ_1 dJ_2, \tag{35}$$

where $U_{\boldsymbol{J}^*}$ is a domain including a vertex at $\boldsymbol{J} = \boldsymbol{J}^*$. Shifting and rescaling J_1 and J_2, we have

$$\varphi(z) = C \int_{U_0} \frac{J_1^{a_1} J_2^{a_2}}{J_1 + J_2 - (z - x_0)} dJ_1 dJ_2, \tag{36}$$

where U_0 is a domain including the shifted vertex at $\boldsymbol{J} = 0$. Using new variables $u = J_1 + J_2$ and $v = J_1 - J_2$,

$$\varphi(z) = \sum_{k,l \geq 0, k+l = a_1+a_2} c_{kl} \int_U \frac{u^k v^l}{u - (z - x_0)} du dv, \tag{37}$$

where c_{kl} is a constant and U is a domain including a vertex at $(u, v) = (0, 0)$. We assume that the line $u = 0$ does not coincide with the boundary of U, since this case results in the line singularity (see section 3.7). As shown in Appendix B, the integral over v yields

$$\varphi(z) = C \int_0^c \frac{u^{1+a_1+a_2}}{u - (z - x_0)} du, \tag{38}$$

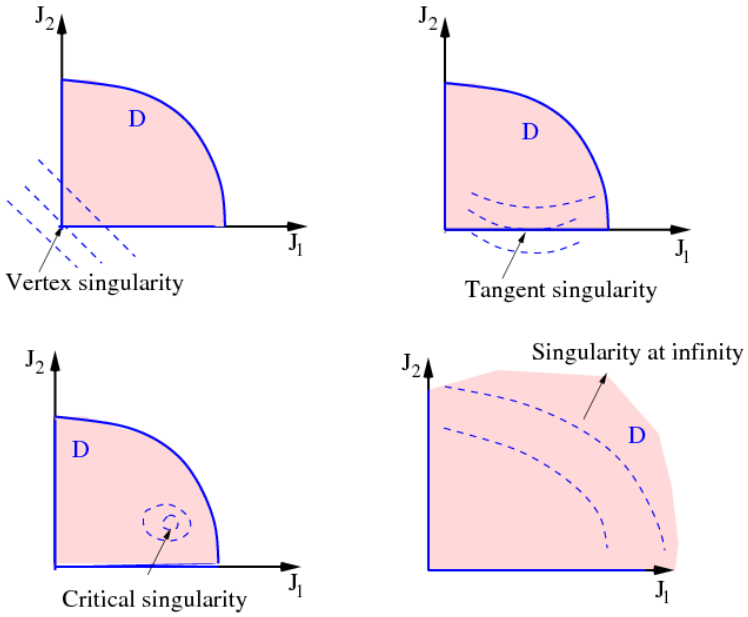

Figure 1. Vertex (top left), tangent (top right), critical (bottom left) singularities, and singularity at infinity (bottom right). In all cases, the domain D is shaded, and the dashed lines are level sets of the function $\mu(\boldsymbol{J})$.

which fits in the framework (E.2). Therefore, the singularity of $\phi(x)$ at $x = x_0$ is:

$$\phi_{x_0}^{\text{sing}}(x) = C_1(x-x_0)^{a_1+a_2+1}\ln|x-x_0| + C_2(x-x_0)^{a_1+a_2+1}H(x-x_0), \quad (39)$$

where H is the Heaviside step function.

3.4. Tangent singularity

We consider now a regular point $\boldsymbol{J}^*$ on the boundary of the domain D such that the level set $\mu(\boldsymbol{J}) = \mu(\boldsymbol{J}^*) = x_0$ is tangent to the boundary of D at $\boldsymbol{J} = \boldsymbol{J}^*$; see figure 1. The appearance of a tangent singularity requires that one derivative of μ vanishes, at a point located on the boundary of D. Changing variables, we may assume that the boundary of D is locally parametrized as $J_2 = J_2^*$; then the tangency condition reads

$$\left.\frac{\partial\mu}{\partial J_1}\right|_{\boldsymbol{J}=\boldsymbol{J}^*} = 0, \quad \boldsymbol{J}^* \in \partial D \quad (40)$$

and at leading order we will use

$$\mu(\boldsymbol{J}) \simeq x_0 + \frac{1}{2}\mu_{11}(J_1 - J_1^*)^2 + \mu_2(J_2 - J_2^*). \quad (41)$$

Using also the leading order approximation (34) for ν, and introducing these into (30), we obtain after shifting and scaling J_1 and J_2 the reduced expression for $\varphi(z)$:

$$\varphi(z) = C\int_U \frac{J_1^{a_1}J_2^{a_2}}{J_1^2 + J_2 - (z-x_0)}dJ_1dJ_2 \quad (42)$$

where the new tangent point is $\boldsymbol{J}^* = (0,0)$, and we have chosen a subdomain U close to $\boldsymbol{J}^*$. Changing variables again and performing one integration, the function φ is further reduced to

$$\varphi(z) = C(1-(-1)^{1+a_1}) \int_0^c \frac{u^{1/2+a_1/2+a_2}}{u-(z-x_0)} du, \tag{43}$$

see Appendix C for details. This form fits in the framework (E.2); hence the singularity of ϕ is:

$$\phi_{x_0}^{\text{sing}}(x) = \begin{cases} C_1(x-x_0)^{1/2+a_1/2+a_2} H(x-x_0) & \\ \quad +C_2(x_0-x)^{1/2+a_1/2+a_2} H(x_0-x) & a_1\text{: even} \\ 0 & a_1\text{: odd.} \end{cases} \tag{44}$$

3.5. Critical singularity

We consider now a point $\boldsymbol{J}^*$ belonging to the interior of D such that the level set $\mu(\boldsymbol{J}) = \mu(\boldsymbol{J}^*) = x_0$ is singular at $\boldsymbol{J}^*$; this requires that both derivatives of μ vanish at $\boldsymbol{J}^*$. In addition, we assume that this critical point is generic, thus the Hessian at $\boldsymbol{J}^*$ has both eigenvalues different from 0. We also discard as non-generic the situation where the critical point $\boldsymbol{J}^*$ belongs to the boundary of D; see an illustration on figure 1. The critical point may be a local extremum or a saddle point. We study both cases in Appendix D, and summarize the results here. Using the leading order approximation (34) for ν, changing variables and performing one integration, the function $\varphi(z)$ is reduced to

$$\varphi(z) = C \int_0^c \frac{u^{(a_1+a_2)/2}}{u-(z-x_0)} du \tag{45}$$

for a local extremum, and to

$$\varphi(z) = C \int_{-c}^c \frac{u^{(a_1+a_2)/2} \ln|u|}{u-(z-x_0)} du \tag{46}$$

for a saddle point. We note that these expressions are valid for even a_1 and a_2, and no singularity appears otherwise. These functions fit into (E.2) and (E.3) respectively, and, for both extremum and saddle points, the singularity of ϕ is:

$$\phi_{x_0}^{\text{sing}}(x) = \begin{cases} C_1(x-x_0)^{(a_1+a_2)/2} \ln|x-x_0| & \\ \quad +C_2(x-x_0)^{(a_1+a_2)/2} H(x-x_0) & a_1, a_2 : \text{even} \\ 0 & \text{otherwise.} \end{cases} \tag{47}$$

3.6. Singularity "at infinity"

Assume $\mu(\boldsymbol{J})$ tends to 0 when $|\boldsymbol{J}|$ tends to infinity; then $x_0 = 0$ is a singular point for $\phi(x)$, see figure 1. This is a common situation for spherical self-gravitating systems. To study this singularity, we assume that the domain D is $[0,+\infty) \times [0,+\infty)$, and

$$\mu(\boldsymbol{J}) \sim (J_1+J_2)^{-a} \ , \ \nu(\boldsymbol{J}) \sim (J_1+J_2)^{-b}. \tag{48}$$

We assume that both a and b are integers with $b > 2$ to ensure convergence of the integrals in (30).

Changing variables to $u = J_1 + J_2$, $v = J_1 - J_2$, and then from u to $s = C_2'/u^a$, we obtain

$$\varphi(z) = C_1' \int_\varepsilon^{+\infty} du \int_{-u}^{u} dv \frac{u^{-b}}{C_2' u^{-a} - (z - x_0)} \tag{49}$$

$$= C_1'' \int_0^c \frac{s^{(b-2)/a-1}}{s - (z - x_0)} ds. \tag{50}$$

The integral over s fits in the framework (E.2), and the leading singularity of ϕ at x_0 is:

$$\phi_{x_0}^{\text{sing}}(x) = \begin{cases} C_1 (x - x_0)^{(b-2)/a-1} \ln|x - x_0| \\ \quad + C_2 (x - x_0)^{(b-2)/a-1} H(x - x_0) & b - 2 \equiv 0 \pmod a \\ C_1 (x - x_0)^{(b-2)/a-1} H(x - x_0) \\ \quad + C_2 (x_0 - x)^{(b-2)/a-1} H(x_0 - x) & b - 2 \not\equiv 0 \pmod a. \end{cases} \tag{51}$$

We will find this kind of singularity in a model of self-gravitating systems, see section 7.

3.7. Line singularity

We consider now a case which seems at first sight very special, but which does occur generically in spherical self-gravitating systems. In a spherical potential, the orbit of a particle with angular momentum $L = 0$ is purely radial; for small L, it is very elongated, and remains close to be purely radial. When the particle travels from one maximal radius to the next along the elongated orbit, this corresponds to one radial period; this also corresponds approximately to a half angular period, see figure 2. Thus, on the $L = 0$ line, the radial frequency is exactly twice the angular frequency $\boldsymbol{\Omega}_r = 2\boldsymbol{\Omega}_\theta$; or equivalently $\boldsymbol{m} \cdot \boldsymbol{\Omega} = 0$, with $\boldsymbol{m} = (1, -2)$.

To study this singularity, we consider a domain D as in figure 2: the axis $J_1 = 0$ is a boundary. Suppose that the function $\mu(\boldsymbol{J})$ is constant on the J_2 axis as

$$\mu(0, J_2) = \text{const.} = x_0 \ , \ \forall J_2 \geq 0. \tag{52}$$

We then expect a singularity of $\phi(x)$ at $x = x_0$. Close to the singular line $J_1 = 0$, we expand $\mu(\boldsymbol{J})$:

$$\mu(\boldsymbol{J}) = x_0 + W(J_2) J_1 + \dots \tag{53}$$

Always having in mind self-gravitating systems, we assume that it is possible to expand ν close to the J_2 axis as:

$$\nu(\boldsymbol{J}) \sim h(J_2) J_1^{a_1} \tag{54}$$

with a non-negative integer a_1. The function φ around $z = x_0$ reads

$$\varphi(z) = \int_0^\varepsilon dJ_1 \int_0^A dJ_2 \frac{h(J_2) J_1^{a_1}}{W(J_2) J_1 - (z - x_0)} \tag{55}$$

$$= \int_0^A dJ_2 \frac{h(J_2)}{W(J_2)^{1+a_1}} \int_0^{\varepsilon / W(J_2)} \frac{u^{a_1} du}{u - (z - x_0)}. \tag{56}$$

The integral over u fits in the framework (E.2); we conclude that the singularity of ϕ at x_0 is:

$$\phi_{x_0}^{\text{sing}}(x) = C_1 (x - x_0)^{a_1} \ln|x - x_0| + C_2 (x - x_0)^{a_1} H(x - x_0). \tag{57}$$

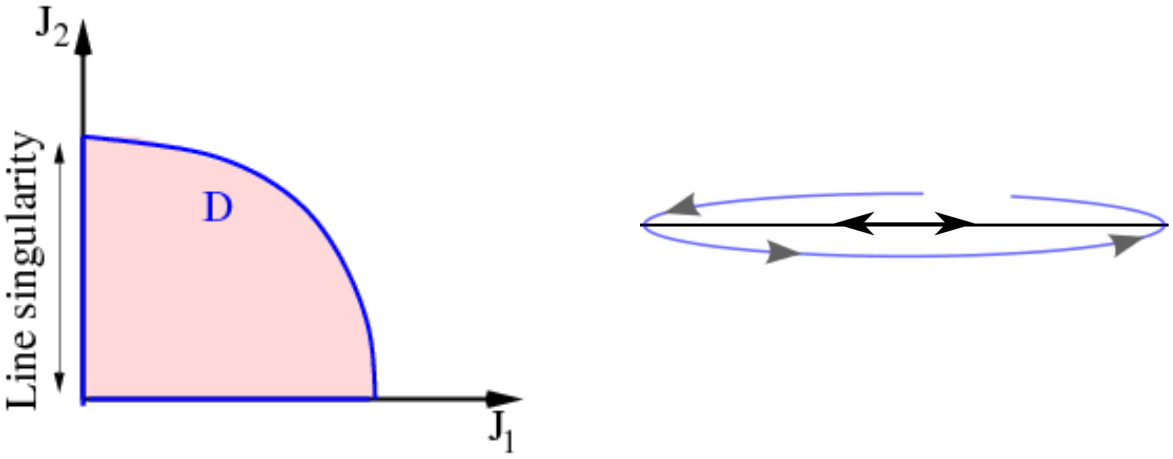

Figure 2. Left: schematic picture of a line singularity. Right: orbits of a particle in a spherical potential with $L = 0$ (black line) and L small (blue elongated orbit).

This computation relies on the fact that $W(J_2)$ is well behaved (for instance bounded away from 0 and ∞).

4. Asymptotic behaviour of a perturbation

The singularities in the functions F and G are passed on to the coefficients $\tilde{a}_k(\omega)$. Each singularity corresponds to a decaying term in the inverse Laplace transform. If $\tilde{a}_k(\omega)$ had a finite number of singularities, the asymptotic in time behaviour of $a_k(t)$ would be a sum of decaying terms, each one corresponding to a singularity of $\tilde{a}_k(\omega)$ (see Theorem 19 in [24]). We expect that this remains true in our situation, where $\tilde{a}_k(\omega)$ actually has an infinite number of singularities.

According to the analysis of section 3 the singular part of $\tilde{a}_k(\omega)$ (or rather of its analytic continuation on the real axis) close to a singular value ω_0 is, for $\omega > \omega_0$:

$$\begin{aligned} &(\omega-\omega_0)^n \ln|\omega-\omega_0| \quad \text{for } n \in \mathbb{Z}_+, \\ \text{or } &(\omega-\omega_0)^a H(\omega-\omega_0) \quad \text{for } a \in \mathbb{R}\setminus\mathbb{Z}. \end{aligned}$$

Here $\mathbb{Z}_+$ is the set of non-negative integers. The behaviour is of course similar for $\omega < \omega_0$. If a function ϕ presents any of the above singularities, we associate to it an asymptotic behaviour of its inverse Laplace transform $\check{\phi}$, according to the following rules [24]:

$$\phi^{\rm sing}_{\omega_0}(\omega) = C(\omega-\omega_0)^n \ln|\omega-\omega_0| \ (n\in\mathbb{Z}_+) \quad \to \check{\phi}^{\rm as}(t) = C' \frac{e^{-i\omega_0 t}}{t^{n+1}} \ , \tag{58}$$

$$\phi^{\rm sing}_{\omega_0}(\omega) = C(\omega-\omega_0)^a H(\omega-\omega_0) \ (a\in\mathbb{R}\setminus\mathbb{Z}) \to \check{\phi}^{\rm as}(t) = C' \frac{e^{-i\omega_0 t}}{t^{a+1}} \ . \tag{59}$$

Singularities and associated asymptotic behaviour are summarized in Table 2. Thus, to extract the asymptotic behaviour of $a_k(t)$, one needs to

(i) Enumerate the singularities appearing in $\tilde{a}_k(\omega)$

(ii) Keep the strongest singularity, corresponding to the slowest decay

(iii) Check if the symmetries of the problem induce a special cancellation.

Unless a cancellation occurs, this strongest singularity yields the decay exponent and asymptotic frequency of $a_k(t)$. We illustrate this strategy on several examples in the following sections, including the case of a cancellation; a careful reexamination of the singularity is then needed.

Type		**Singularity**	**Exponent** α	**Damping**	**Sign**
Vertex		(E.4)	$1+a_1+a_2$	$e^{-ix_0t}t^{-(2+a_1+a_2)}$	$(-1)^{1+\alpha}$
Tangent	(a_1 : even)	(E.5)	$1/2+a_1/2+a_2$	$e^{-ix_0t}t^{-(3/2+a_1/2+a_2)}$	—
	(a_1 : odd)	N/A	N/A	N/A	
Critical					
extremum	(a_1, a_2 : even)	(E.4)	$(a_1+a_2)/2$	$e^{-ix_0t}t^{-(1+(a_1+a_2)/2)}$	$(-1)^{1+\alpha}$
saddle	(a_1, a_2 : even)	(E.6)	$(a_1+a_2)/2$	$e^{-ix_0t}t^{-(1+(a_1+a_2)/2)}$	$(-1)^{\alpha}$
	(otherwise)	N/A	N/A	N/A	
Infinity	($(b-2)/a \in \mathbb{Z}$)	(E.4)	$(b-2)/a-1$	$e^{-ix_0t}t^{-(b-2)/a}$	$(-1)^{1+\alpha}$
	($(b-2)/a \notin \mathbb{Z}$)	(E.5)	$(b-2)/a-1$	$e^{-ix_0t}t^{-(b-2)/a}$	—
Line		(E.4)	a_1	$e^{-ix_0t}t^{-(1+a_1)}$	$(-1)^{1+\alpha}$

Table 2. Table of singularities of the function $\phi(x)$ defined by (30) and (31), with their associated exponent α (see section 3 and Appendix E), and asymptotic dampings. The singularity is produced at $\boldsymbol{J}^* = (J_1^*, J_2^*)$, and $x_0 = \mu(J_1^*, J_2^*)$. The leading order of the numerator is $\nu(\boldsymbol{J}) \simeq (J_1 - J_1^*)^{a_1}(J_2 - J_2^*)^{a_2}$ for vertex, tangent and critical singularities, $\nu(\boldsymbol{J}) \simeq (J_1+J_2)^{-b}$ for a singularity at infinity, and $\nu(\boldsymbol{J}) \simeq h(J_2)J_1^{a_1}$ for a line singularity. We assume $\mu(\boldsymbol{J}) \simeq (J_1+J_2)^{-a}$ for a singularity at infinity. a_1 and a_2 are non-negative integers, a is an integer and b is an integer satisfying $b > 2$. N/A means that no singularity appears in $\phi(x)$. This table shows the leading singularity for each type. As shown in sections 6 and 7, a special cancellation for the leading term may happen between modes $\boldsymbol{m}$ and $-\boldsymbol{m}$. The column Sign represents the relative sign between the singular parts of modes $\boldsymbol{m}$ and$-\boldsymbol{m}$ for $x_0 = 0$. No cancellation is expected for $x_0 \neq 0$ irrespective of the relative sign. A bar means no simple relation between the two modes. Note that the relative sign may also depend on the numerator $\nu(\boldsymbol{J})$ of (30) if it depends on $\boldsymbol{m}$, but this dependence is ignored in this table.

A remark is in order: we study here the asymptotic behaviour of the $a_k(t)$, which are the coefficients of the density and potential perturbation in the expansions (19) and (20). One might expect that the slowest decay for these coefficients yields the asymptotic decay of the density or potential perturbation at a given point in space. This is not necessarily true, as we have no information on the rate at which a_k reaches its asymptotic regime, and thus have no control on the series (19) and (20).

5. Preparation for numerical tests

5.1. On numerical tests

The theory developed in this paper should describe the asymptotic behaviour of a perturbation evolving according to the linearized Vlasov equation. Two questions arise:

i) Since the above computations are formal, one may wonder if the theory is correct for the evolution of a linearized Vlasov equation.
ii) Even if the theory is correct for the linearized Vlasov equation, it is not clear that it describes the asymptotic behaviour of the fully non-linear Vlasov equation.
To answer these questions, direct numerical simulations of the Vlasov equation are required. Such a check has been done in a one-dimensional setting using N-body simulations [22]; however, the memory, accuracy and time frame required to perform similar simulations in two or more spatial dimensions make the task challenging. Instead, we will illustrate the various aspects of the theory on much simpler linear advection equations in section 6, and apply it to make definite predictions on a spherically symmetric self-gravitating system in section 7.

5.2. Advection equation and singularity analysis

To illustrate the theory, we consider an advection equation

$$\partial_t f + \boldsymbol{\Omega}(\boldsymbol{J}) \cdot \nabla_{\boldsymbol{\theta}} f = 0. \tag{60}$$

The exact solution is

$$f(\boldsymbol{\theta}, \boldsymbol{J}, t) = f(\boldsymbol{\theta} - \boldsymbol{\Omega}(\boldsymbol{J})t, \boldsymbol{J}, t = 0). \tag{61}$$

We consider the temporal evolution of the expected value of $A(\boldsymbol{\theta})$ defined by

$$\langle A \rangle (t) = \int A(\boldsymbol{\theta}) f(\boldsymbol{\theta}, \boldsymbol{J}, t) d\boldsymbol{\theta} d\boldsymbol{J}, \tag{62}$$

where f is governed by the advection equation (60) and we assumed that A is a function of $\boldsymbol{\theta}$ only. From the Fourier-Laplace transform of the advection equation (60), the Laplace transform of $\langle A \rangle (t)$ is given by

$$\widetilde{\langle A \rangle}(\omega) = \sum_{\boldsymbol{m}} \int A(\boldsymbol{\theta}) e^{i\boldsymbol{m}\cdot\boldsymbol{\theta}} d\boldsymbol{\theta} \int \frac{g(\boldsymbol{m}, \boldsymbol{J})}{\boldsymbol{m} \cdot \boldsymbol{\Omega}(\boldsymbol{J}) - \omega} d\boldsymbol{J}, \tag{63}$$

where $ig(\boldsymbol{m}, \boldsymbol{J})$ is the Fourier transform of $f(\boldsymbol{\theta}, \boldsymbol{J}, t = 0)$. The function

$$\varphi(\omega; \boldsymbol{m}) = \int \frac{g(\boldsymbol{m}, \boldsymbol{J})}{\boldsymbol{m} \cdot \boldsymbol{\Omega}(\boldsymbol{J}) - \omega} d\boldsymbol{J} \tag{64}$$

fits in the framework (30), thus the asymptotic damping of the expected value $\langle A \rangle (t)$ is predicted by the theory presented in sections 3 and 4.

The theoretically predicted asymptotic damping can be checked without computing the temporal evolution of f numerically, since we have the exact solution (61) to the advection equation, which gives

$$\langle A \rangle (t) = \sum_{\boldsymbol{m}} \int A(\boldsymbol{\theta}) e^{i\boldsymbol{m}\cdot\boldsymbol{\theta}} d\boldsymbol{\theta} \int ig(\boldsymbol{m}, \boldsymbol{J}) e^{-i\boldsymbol{m}\cdot\boldsymbol{\Omega}(\boldsymbol{J})t} d\boldsymbol{J}. \tag{65}$$

Integrals over $\boldsymbol{\theta}$ can be performed analytically, and hence our numerical task is to perform integrals over $\boldsymbol{J}$. Consequently, we can reduce the $2d$-dimensional problem (60) to d-dimensional integrals over $\boldsymbol{J}$. For 2-dimensional cases, numerical integrations are possible with good accuracy.

6. Numerical tests

We set the initial distribution as

$$f(\boldsymbol{\theta}, \boldsymbol{J}, t=0) = J_1^{h_1} J_2^{h_2} (J_1 - J_1^*)^{a_1} (J_2 - J_2^*)^{a_2} e^{-(J_1^2+J_2^2)/2} (1+\cos\theta_1 \cos\theta_2), \quad (66)$$

where the unity is to keep f positive, but is not important since the mode $(0,0)$ is temporally invariant. We therefore focus on the four modes $\boldsymbol{m} = (1,1), (1,-1), (-1,1)$ and $(-1,-1)$. We assume that the system is defined on the domain $(J_1, J_2) \in [0, +\infty)^2$. The factor $(J_1 - J_1^*)^{a_1} (J_2 - J_2^*)^{a_2}$ corresponds to the leading estimation of $\nu(J)$ (34), and the factor $J_1^{h_1} J_2^{h_2}$ will be used to select the singularities we want to illustrate. The function g is the same for the four modes and, remembering ig is the Fourier transform of the initial perturbation,

$$ig(\boldsymbol{m}, \boldsymbol{J}) = \frac{1}{4} J_1^{h_1} J_2^{h_2} (J_1 - J_1^*)^{a_1} (J_2 - J_2^*)^{a_2} e^{-(J_1^2+J_2^2)/2}, \quad \boldsymbol{m} = (\pm 1, \pm 1). \quad (67)$$

We introduce four observables:

$$A_1 = \cos(\theta_1+\theta_2),\ A_2 = \sin(\theta_1+\theta_2),\ A_3 = \cos(\theta_1-\theta_2),\ A_4 = \sin(\theta_1-\theta_2), \quad (68)$$

to pick up singularities appearing in the modes $(1,1)$ and $(-1,-1)$ by A_1 and A_2, and in the modes $(1,-1)$ and $(-1,1)$ by A_3 and A_4.

We now report detailed theoretical predictions and numerical illustrations for vertex, tangent and critical singularities in sections 6.1, 6.2 and 6.3 respectively. These include cases with cancellations between two modes. The line singularity is discussed in section 6.4 on a toy model, which also has the vertex and tangent singularities. We discuss the dominant singularity for different modes, again taking into account cancellations, and check the predictions against numerical computations. The singularity at infinity will be demonstrated in section 7 on a spherical self-gravitating model.

In this section, all the numerical integrations for the exact expected values are performed by introducing a cutoff at $J_1 = J_2 = 10$ and slicing the interval $[0, 10]$ in 2^{12} bins.

6.1. Vertex singularity

We set the frequencies as

$$\Omega_1(\boldsymbol{J}) = J_1, \quad \Omega_2(\boldsymbol{J}) = J_2, \quad (69)$$

which yields a vertex singularity at the origin, with $(J_1^*, J_2^*) = (0,0)$; the associated frequency is $\omega_0 = \boldsymbol{m} \cdot \boldsymbol{\Omega}(\boldsymbol{J}^*) = 0$. We compute $\langle A_i \rangle(t)$ for $a_1 = 0, 1$ and 2 with fixed $a_2 = 0$. There are no singularities of other types, thus we may use $h_1 = h_2 = 0$. From Table 2, we predict dampings and cancellations as shown in Table 3. Cancellations occur for A_1 and A_3 with an odd a_1, since the cosine observables pick up the sum of the modes $\boldsymbol{m}$ and $-\boldsymbol{m}$; for instance:

$$A_1 = \cos(\theta_1 + \theta_2) \quad \Longrightarrow \quad \widetilde{\langle A_1 \rangle}(\omega) \propto \varphi(\omega; (1,1)) + \varphi(\omega; (-1,-1)), \quad (70)$$

(a_1, a_2)	$(0,0)$	$(1,0)$	$(2,0)$
$\langle A_1 \rangle (t)$	t^{-2}	C	t^{-4}
$\langle A_2 \rangle (t)$	C	t^{-3}	C
$\langle A_3 \rangle (t)$	t^{-2}	C	t^{-4}
$\langle A_4 \rangle (t)$	C	t^{-3}	C

Table 3. Dampings and cancellations for the vertex singularity. "C" stands for "cancellation".

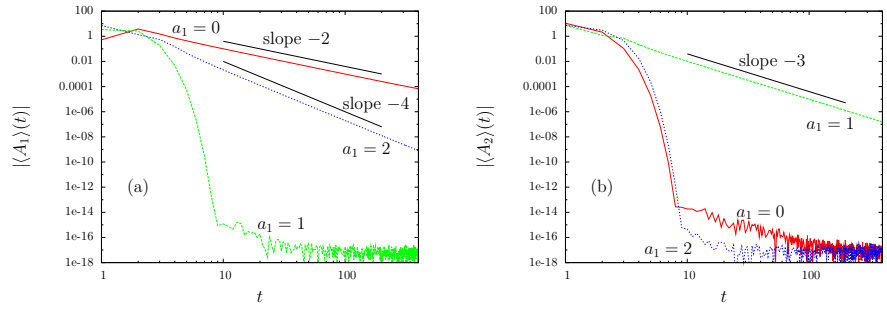

Figure 3. Dampings for the vertex singularity. Observables are (a) A_1 and (b) A_2. The parameter a_2 is fixed as 0. Observables A_3 and A_4 give qualitatively similar panels to A_1 and A_2 respectively.

and $\varphi(\omega; (-1,-1)) = (-1)^{a_1+a_2}\varphi(\omega; (1,1))$ holds for the vertex singularity. Similarly, cancellations occur for the sine observables A_2 and A_4 with an even a_1 since, for instance,

$$A_2 = \sin(\theta_1 + \theta_2) \quad \Longrightarrow \quad \widetilde{\langle A_2 \rangle}(\omega) \propto \varphi(\omega; (1,1)) - \varphi(\omega; (-1,-1)). \quad (71)$$

We note that the cancellations occur for the leading singularities; higher-order singularities may survive in general. However, in this case, higher-order singularities coming from the expansion of $\exp(-(J_1^2 + J_2^2)/2)$ do not change the parity of $a_1 + a_2$, since expanded terms consist of J_1^2 and J_2^2. Thus, all orders are cancelled when the leading order is cancelled.

The above prediction is confirmed by direct numerical integration of (65) as shown in figure 3. We remark that dampings without oscillation reflect the zero frequency $\omega_0 = 0$. We have also checked that no cancellation occurs when we replace Ω_1 by $\Omega_1(\boldsymbol{J}) = J_1 + 1$, since $\omega_0 = 1 \neq 0$ (figure not shown).

6.2. Tangent singularity

We set the frequencies as

$$\Omega_1(\boldsymbol{J}) = (J_1 - 1)^2, \quad \Omega_2(\boldsymbol{J}) = J_2. \quad (72)$$

There are a vertex singularity at $(J_1, J_2) = (0,0)$ and a tangent singularity at $(J_1, J_2) = (1,0)$. We are interested in the tangent singularity, and hence we set $(J_1^*, J_2^*) = (1,0)$ which gives the frequency $\omega_0 = 0$. We choose a_1 and a_2 from the set $\{0,1,2\}$, and use $h_1 = 2$ and $h_2 = 0$ to hide the vertex singularity: the slowest decay coming from

the vertex singularity is then t^{-4}. The predicted dampings and cancellations are shown in Table 4. An explanation is needed for the case $(a_1, a_2) = (1, 0)$: the leading order does not give any singularity, since a_1 is odd; however, expanding $ig(\boldsymbol{m}, \boldsymbol{J})$ around $(J_1^*, J_2^*) = (1, 0)$, the second leading order gives $a_1 = 2$; thus the damping must be $t^{-2.5}$, as in the case $(a_1, a_2) = (2, 0)$. We remark that no cancellation occurs for the tangent singularities. These predictions have been checked numerically, though no figures are reported.

(a_1, a_2)	$(0,0)$	$(0,1)$	$(0,2)$	$(1,0)$	$(2,0)$
$\langle A_i \rangle (t)$	$t^{-1.5}$	$t^{-2.5}$	$t^{-3.5}$	$t^{-2.5}$	$t^{-2.5}$

Table 4. Dampings and cancellations for the tangent singularity.

6.3. Critical singularity

We set the frequencies as

$$\Omega_1(\boldsymbol{J}) = (J_1 - 1)^2, \quad \Omega_2(\boldsymbol{J}) = (J_2 - 1)^2. \tag{73}$$

Singularities are: a vertex singularity at $(J_1, J_2) = (0, 0)$, tangent singularities at $(J_1, J_2) = (1, 0)$ and $(0, 1)$, and a critical singularity at $(J_1, J_2) = (1, 1)$. We are now interested in the critical singularity, and hence we set $(J_1^*, J_2^*) = (1, 1)$ giving the frequency $\omega_0 = 0$. We choose a_1 from the set $\{0, 1, 2\}$, and use $h_1 = h_2 = 2$ to hide the vertex and tangent singularities as done in section 6.2.

Cancellations between the modes $\boldsymbol{m}$ and $-\boldsymbol{m}$ are as follows. We first remark that no leading singularity appears for $(a_1, a_2) = (1, 0)$ since a_1 is odd. In this case, as discussed in the case of the tangent singularity, the second leading singularity gives the same singularity as $(a_1, a_2) = (2, 0)$, thus we concentrate on $(a_1, a_2) = (0, 0)$ and $(2, 0)$. The second remark is that the critical singularity at $(J_1, J_2) = (1, 1)$ behaves as an extremum singularity for A_1 and A_2, and as a saddle singularity for A_3 and A_4. Referring to Table 2 and the above second remark, the leading singularities in A_1 and A_4 are cancelled for $(a_1, a_2) = (0, 0)$, and in A_2 and A_3 for $(a_1, a_2) = (2, 0)$. In the latter case, the next leading singularities come from $(a_1, a_2) = (4, 0)$ for instance, and t^{-3} dampings are predicted. These discussions are summarized in Table 5.

We explain the whole cancellation in $\langle A_4 \rangle (t)$ for $(a_1, a_2) = (0, 0)$. The exact solution of $\langle A_4 \rangle (t)$ is proportional to

$$\langle A_4 \rangle (t) = C \int g(J_1, J_2) \sin((\Omega_1(J_1, J_2) - \Omega_2(J_1, J_2))t) d\boldsymbol{J}. \tag{74}$$

Exchanging the dummy variables J_1 and J_2, and using invariance of g under this exchange, we have $\langle A_4 \rangle (t) = 0$. From the view point of singularity analysis, using notations of Appendix D and Appendix E, the invariance of g with respect to the exchange between J_1 and J_2 implies that the numerator of the integrand in (E.3) is of the type $u^\alpha \ln |u|$ with even α, since $u = J_1^2 - J_2^2$. The evenness of α gives the

(a_1, a_2)	$(0,0)$	$(1,0)$	$(2,0)$
$\langle A_1 \rangle (t)$	t^{-2}(C)	t^{-2}(N)	t^{-2}
$\langle A_2 \rangle (t)$	t^{-1}	t^{-3}(N)	t^{-3}(C)
$\langle A_3 \rangle (t)$	t^{-1}	t^{-3}(N)	t^{-3}(C)
$\langle A_4 \rangle (t)$	C	t^{-2}(N)	t^{-2}

Table 5. Dampings and cancellations for the critical singularity. "C" means that there is a cancellation at leading order, and "N" that the leading order singularity does not exist. Dampings associated with the next leading singularities are observed when "C" or "N" appears. In $\langle A_4 \rangle (t)$ for $(a_1, a_2) = (0,0)$, all the singularities at any orders are cancelled due to a special symmetry of $g(\boldsymbol{m}, \boldsymbol{J})$.

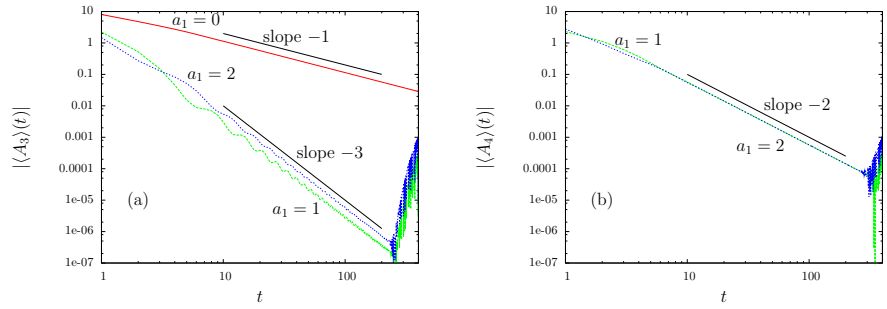

Figure 4. Dampings for the critical singularity. Observables are (a) A_3 and (b) A_4. The parameter a_2 is fixed as 0. The curves for $a_1 = 1$ and 2 in (b) are almost superposed. The curve of $a_1 = 0$ in (b) is out of range due to a special cancellation. Except for this special cancellation, A_1 and A_2 give qualitatively similar panels to A_4 and A_3 respectively.

same sign for the two modes $\boldsymbol{m}$ and $-\boldsymbol{m}$ in the saddle singularity, hence they cancel each other in the sine observable A_4: this is of course compatible with the exact result $\langle A_4 \rangle (t) = 0$.

6.4. Toy model

We set the frequencies as

$$\Omega_1(\boldsymbol{J}) = -J_1 - \frac{J_1^2}{2} - 2J_2, \quad \Omega_2(\boldsymbol{J}) = -2J_1 + 2J_2. \tag{75}$$

This toy model (75) has three types of singularities:

- Vertex singularity at $(J_1^*, J_2^*) = (0,0)$ for the modes $(1,-1)$ and $(-1,1)$.
- Tangent singularity at $(J_1^*, J_2^*) = (1,0)$ for the modes $(1,-1)$ and $(-1,1)$.
- Line singularity on the J_2 axis for the modes $(1,1)$ and $(-1,-1)$.

No critical singularity and no singularity at infinity appear. We use distribution (66), with $h_1 = h_2 = a_1 = a_2 = 0$, that is

$$ig(\boldsymbol{m}, \boldsymbol{J}) = e^{-(J_1^2 + J_2^2)/2}. \tag{76}$$

Singularity	**Vertex**	**Tangent**	**Line(leading)**	**Line(second)**
Damping	t^{-2}	$e^{-it/2}t^{-1.5}$	t^{-1}	t^{-2}
Modes	$(\pm1,\mp1)$	$(\pm1,\mp1)$	$(\pm1,\pm1)$	$(\pm1,\pm1)$
(J_1^*, J_2^*)	$(0,0)$	$(1,0)$	J_2 axis	J_2 axis
$A_1 = \cos(\theta_1+\theta_2)$	N/A	N/A	C	D
$A_2 = \sin(\theta_1+\theta_2)$	N/A	N/A	D	C
$A_3 = \cos(\theta_1-\theta_2)$	E	D	N/A	N/A
$A_4 = \sin(\theta_1-\theta_2)$	C	D	N/A	N/A

Table 6. Theoretical prediction of the asymptotic damping for the A_i observables in the toy model (75). "D" indicates the dominant singularity, "E" an existing but subdominant singularity, and "C" a cancelled singularity. "N/A" tells that the corresponding singularity cannot be captured by the observable. An oscillation is predicted for the tangent singularity only.

6.4.1. Cancellation and higher-order contribution Three different types of singularities appear for the A_i observables, the strongest of which is a line singularity, see Table 6. Concentrating on A_1 and A_2, we show an example of cancellation for this line singularity.

The relative sign between $\varphi(\omega;\boldsymbol{m})$ and $\varphi(\omega;-\boldsymbol{m})$ is $(-1)^{1+a_1}$ for the line singularity. Thus, the leading singularity corresponding to $a_1=0$ is cancelled for A_1 but not for A_2.

Higher-order singularities may come from the expansion of g around $J_1=0$ and correspond to $a_1\geq 1$. However, since g is even in J_1, the same cancellation will take place at all orders. Consequently, there is no higher-order contribution from g.

Nevertheless, a higher-order contribution comes from $\boldsymbol{m}\cdot\boldsymbol{\Omega}(\boldsymbol{J})$. For the mode $\boldsymbol{m}=(1,1)$, the function $\varphi(\omega;\boldsymbol{m})$ becomes

$$\varphi(\omega;(1,1)) \simeq \frac{1}{4i}\int_0^\epsilon \frac{dJ_1}{-3J_1-J_1^2/2-\omega}\int_0^C dJ_2 = \frac{C}{4i}\int_0^\epsilon \frac{dJ_1}{-3J_1-J_1^2/2-\omega} \quad (77)$$

keeping the leading order of $g(\boldsymbol{m},\boldsymbol{J})$, which is constant. Changing variable from J_1 to $u=3J_1+J_1^2/2$, we have

$$\begin{aligned}\varphi(\omega;(1,1)) &= \frac{-C}{12i}\int_0^{\epsilon'}\frac{(1+2u/9)^{-1/2}}{u+\omega}du = \frac{-C}{12i}\int_0^{\epsilon'}\frac{1-u/9+O(u^2)}{u+\omega}du \\ &\simeq \frac{-C}{12i}\left[-\ln|\omega| - \frac{\omega}{9}\ln|\omega| + \cdots\right]. \quad (78)\end{aligned}$$

A similar computation gives

$$\varphi(\omega;(-1,-1)) \simeq \frac{-C}{12i}\left[\ln|\omega| - \frac{\omega}{9}\ln|\omega| + \cdots\right]. \quad (79)$$

Coming back to the expression (70), the leading order $\ln|\omega|$ is cancelled for the observable $A_1=\cos(\theta_1+\theta_2)$. However, the second leading order $\omega\ln|\omega|$ survives, and gives a t^{-2} asymptotic damping.

Similarly, we can find another cancellation for the observable $A_4=\sin(\theta_1-\theta_2)$ on the vertex singularity. From the above discussions, we build Table 6 which summarizes existing, dominant and cancelled singularities for the four observables.

6.4.2. Numerical computations of the exact solution On figure 5, we compare the theoretical prediction of Table 6 with the numerically computed exact temporal evolution of the four observables (68). We examine both amplitude's damping and frequency of $\langle A_j \rangle (t)$, whose exact solution is

$$\langle A_j \rangle (t) = \pi^2 \int_0^\infty \int_0^\infty e^{-(J_1^2+J_2^2)/2} A_j(\Omega_1(\boldsymbol{J})t, \Omega_2(\boldsymbol{J})t) dJ_1 dJ_2 \tag{80}$$

by (65). Temporal evolutions of the four observables are reported in figure 5, and the agreements in damping rates are very good for all observables. Observables A_1 and A_2 have no tangent singularity, and hence the prediction for the frequencies of $\langle A_1 \rangle (t)$ and $\langle A_2 \rangle (t)$ is zero. These zero frequencies are observed in figures 5(a) and (b). On the other hand, the observables A_3 and A_4 are dominated by the tangent singularity at $(J_1^*, J_2^*) = (1, 0)$, and the prediction for the frequencies is $|\Omega_1(1,0) - \Omega_2(1,0)| = 0.5$. Looking at the temporal evolutions in linear scale in figure 6, we see that the predicted frequency is in good agreement with the numerics.

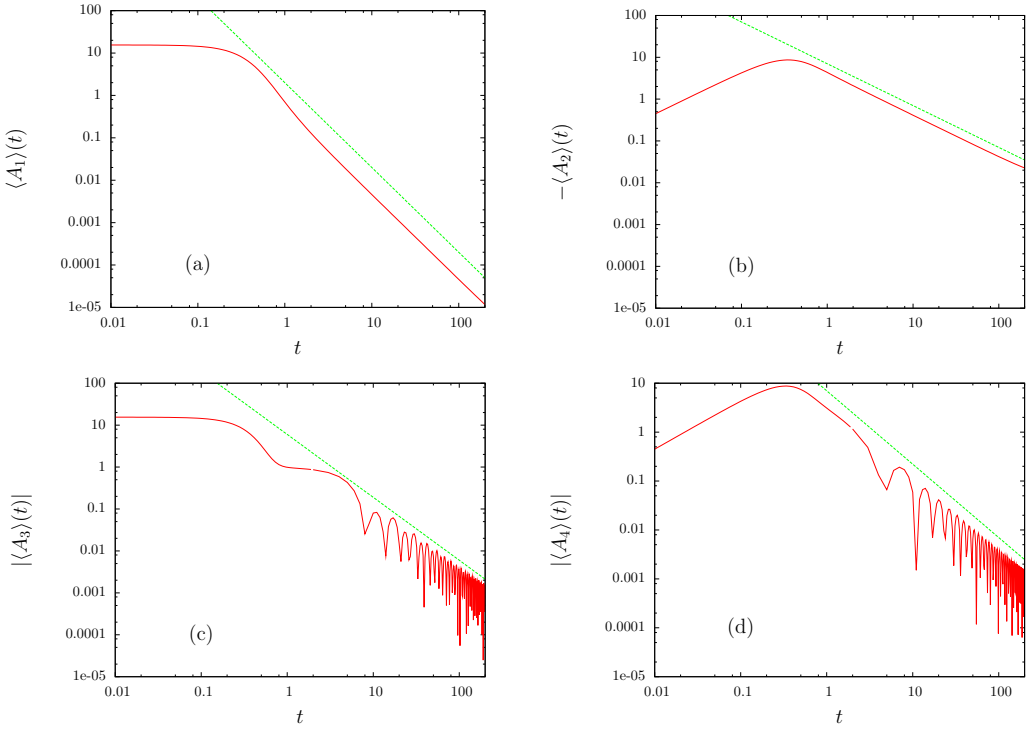

Figure 5. Temporal evolutions of the four observables: (a) $\langle A_1 \rangle (t)$ with $A_1 = \cos(\theta_1 + \theta_2)$. (b) $-\langle A_2 \rangle (t)$ with $A_2 = \sin(\theta_1 + \theta_2)$. (c) $|\langle A_3 \rangle (t)|$ with $A_3 = \cos(\theta_1 - \theta_2)$. (d) $|\langle A_4 \rangle (t)|$ with $A_4 = \sin(\theta_1 - \theta_2)$. All panels have the same scales. Straight lines show the theoretically predicted algebraic dampings, which are respectively $t^{-2}, t^{-1}, t^{-1.5}$ and $t^{-1.5}$. $\langle A_j \rangle (t)$ is computed by using (80) with cutoff at $J_1 = J_2 = 10$.

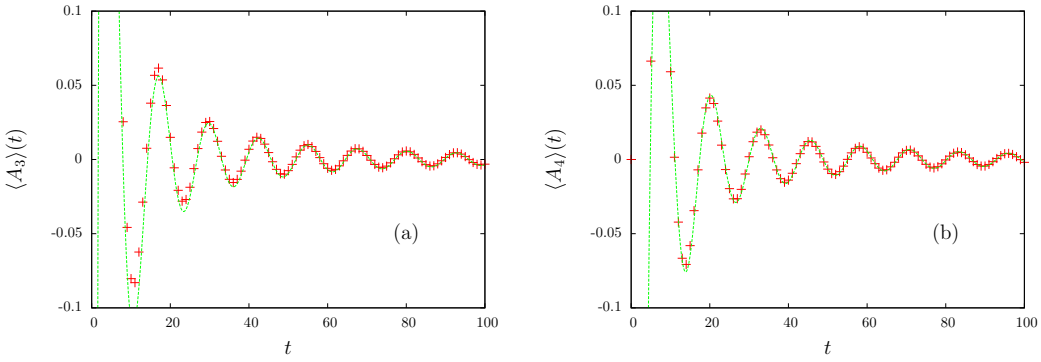

Figure 6. Temporal evolutions of (a) $\langle A_3 \rangle$ and (b) $\langle A_4 \rangle$ in linear scale. Red plus points are numerically obtained, and green lines represent $4t^{-1.5}\cos(0.5(t-4.8))$ and $4t^{-1.5}\cos(0.5(t-8))$ in (a) and (b) respectively.

7. Spherically symmetric stellar system

7.1. Isochrone model

We present the isochrone model, which is a simple example of a spherically symmetric stellar system. The potential of this model is

$$\Phi(r) = -\frac{GM}{b+\sqrt{b^2+r^2}}, \tag{81}$$

where G is the gravitational constant, M is the total mass of the system, and b is a parameter. A stationary state satisfying the self-consistent condition for the potential is known to be [11]:

$$f_0 = \frac{1}{\sqrt{2}(2\pi)^3(GMb)^{3/2}} \frac{\sqrt{\tilde{E}}}{[2(1-\tilde{E})]^4} \left[27 - 66\tilde{E} + 320\tilde{E}^2 - 240\tilde{E}^3 \right.$$
$$\left. +64\tilde{E}^4 + 3(16\tilde{E}^2 + 28\tilde{E} - 9) \frac{\sin^{-1}\sqrt{\tilde{E}}}{\sqrt{\tilde{E}(1-\tilde{E})}} \right], \tag{82}$$

where $\tilde{E} = -Eb/GM$ and E is energy.

Let (r, ϑ, ψ) be the 3-dimensional polar coordinate, and $(J_r, J_\vartheta, J_\psi)$ the conjugate angular momenta. We introduce new actions (J_1, J_2, J_3):

$$J_1 = J_\psi, \quad J_2 = J_\vartheta + |J_\psi|, \quad J_3 = J_r. \tag{83}$$

We denote the conjugate angle variables by $(\theta_1, \theta_2, \theta_3)$. The Hamiltonian of this model is then

$$H(\boldsymbol{J}) = -\frac{(GM)^2}{2[J_3 + \frac{1}{2}(J_2 + \sqrt{J_2^2 + 4GMb})]^2}. \tag{84}$$

The Hamiltonian is defined on the domain $(J_1, J_2, J_3) \in [-J_2, J_2] \times [0, \infty) \times [0, \infty)$. We remark that the Hamiltonian depends on J_2 and J_3, but not on J_1. We hence omit the modes corresponding to J_1, and write $\boldsymbol{m} = (m_2, m_3)$ for the mode vector

and $\boldsymbol{\Omega} = (\Omega_2, \Omega_3)$ for the frequency vector. Thus, the isochrone model fits in the 2-dimensional analysis developed in this paper. Note that for consistency with standard notations, the actions J_2 and J_3 in the isochrone model correspond to J_1 and J_2 in the general theory of section 3. Frequencies are given by

$$\Omega_3(\boldsymbol{J}) = \frac{\partial H}{\partial J_3}(\boldsymbol{J}) = \frac{(GM)^2}{\left[J_3 + \frac{1}{2}(J_2 + \sqrt{J_2^2 + 4GMb})\right]^3}, \tag{85}$$

$$\Omega_2(\boldsymbol{J}) = \frac{\partial H}{\partial J_2}(\boldsymbol{J}) = \frac{1}{2}\left(1 + \frac{J_2}{\sqrt{J_2^2 + 4GMb}}\right)\Omega_3(\boldsymbol{J}). \tag{86}$$

7.2. Advection equation corresponding to isochrone model

Using the frequencies Ω_2 (86) and Ω_3 (85), we consider the advection equation

$$\frac{\partial f_1}{\partial t} + \Omega_2(\boldsymbol{J})\frac{\partial f_1}{\partial \theta_2} + \Omega_3(\boldsymbol{J})\frac{\partial f_1}{\partial \theta_3} = 0. \tag{87}$$

This advection equation is obtained by omitting the potential perturbation in the linearized Vlasov equation. We take as initial state:

$$f(\boldsymbol{\theta}, \boldsymbol{J}, t = 0) = f_0(\boldsymbol{J}) + f_1(\boldsymbol{\theta}, \boldsymbol{J}, t = 0), \tag{88}$$

where $f_0(\boldsymbol{J})$ is the stationary state (82) and the perturbation f_1 is set as

$$f_1(\boldsymbol{\theta}, \boldsymbol{J}, t = 0) = a f_0(\boldsymbol{J}) \cos(n_2\theta_2)\cos(n_3\theta_3), \quad |a| \ll 1. \tag{89}$$

Note that this perturbation is also independent of θ_1 and J_1. The Fourier transform $ig(\boldsymbol{m}, \boldsymbol{J})$ of $f_1(\boldsymbol{\theta}, \boldsymbol{J}, t = 0)$ is then

$$ig(\boldsymbol{m}, \boldsymbol{J}) = \begin{cases} af_0(\boldsymbol{J})/4 & (m_2, m_3) = (\pm n_2, \pm n_3) \\ 0 & \text{otherwise.} \end{cases} \tag{90}$$

Let us consider the temporal evolution of the expected value of an observable $A(\theta_2, \theta_3)$. As discussed in section 5.2, the Laplace transform of the expected value is given by (63), but the integrals should be performed over $\theta_1, \theta_2, \theta_3, J_1, J_2$ and J_3. Remembering that A, f_1 and $\boldsymbol{\Omega}$ do not depend on θ_1 and J_1, the expected value may be written as a linear combination of functions of the form

$$\varphi(\omega; \boldsymbol{m}) = \int_0^\infty dJ_3 \int_0^\infty dJ_2 \, \frac{1}{\boldsymbol{m}\cdot\boldsymbol{\Omega}(\boldsymbol{J}) - \omega} \int_{-J_2}^{J_2} h(\boldsymbol{m}, \boldsymbol{J}) dJ_1. \tag{91}$$

Note that if we were studying the true linearized Vlasov equation, the function h in the above equation would be replaced by $\boldsymbol{m}\cdot\nabla_{\boldsymbol{J}} f_0(\boldsymbol{J})\bar{c}_l(\boldsymbol{m}, \boldsymbol{J})c_k(\boldsymbol{m}, \boldsymbol{J})$ or $g(\boldsymbol{m}, \boldsymbol{J})\bar{c}_l(\boldsymbol{m}, \boldsymbol{J})$, according to the definitions of $F_{lk}(\omega)$ and $G_l(\omega)$ in equations (25) and (26) respectively. Since $\int_{-J_2}^{J_2} h dJ_1$ vanishes for $J_2 = 0$, a J_2 factor can be factorized, and we can write $\int_{-J_2}^{J_2} h(\boldsymbol{m}, \boldsymbol{J}) dJ_1 = J_2\tilde{h}(\boldsymbol{m}, \boldsymbol{J})$. Thus, the functions (91) fit in the framework of the abstract setting (30), and we apply the theory developed in sections 3 and 4, with

$$\nu(\boldsymbol{J}) = J_2\tilde{h}(\boldsymbol{m}, \boldsymbol{J}), \quad \mu(\boldsymbol{J}) = \boldsymbol{m}\cdot\boldsymbol{\Omega}(\boldsymbol{J}). \tag{92}$$

The J_2 factor in $\nu(\boldsymbol{J})$ will be of importance to determine the singularity associated with vertex, line and infinite singularities.

Singularity	**Damping**	**Frequency**	**Condition for mode**
Vertex	t^{-3}	$\left(\frac{m_2}{2}+m_3\right)\frac{\sqrt{GM}}{2^4 b^{3/2}}$	None
Tangent	$t^{-1.5}$	$m_2\Omega_2(J_2^*,0)+m_3\Omega_3(J_2^*,0)$	$-1<m_3/m_2<-1/3$
Line	t^{-2}	0	$m_2=-2m_3$
Infinity	$t^{-2/3}$	0	None

Table 7. Dampings and frequencies associated with singularities in the isochrone model. This table shows the leading singularity for each type. (m_2, m_3) represents a mode. J_2^* is the solution to (94). Modes satisfying $m_2+2m_3=0$ or $m_2+3m_3=0$ do not yield a generic vertex singularity, but a line singularity and a special vertex singularity respectively. See text for the leading line singularity.

7.3. Singularities in isochrone model and theoretical prediction

We can now list the singularities in the isochrone model:

- Vertex singularity at $(J_2^*, J_3^*) = (0,0)$, except for the modes $\boldsymbol{m}$ satisfying $m_2 + 2m_3 = 0$ or $m_2 + 3m_3 = 0$. The former case results in a line singularity, and the latter case gives a special vertex singularity with $\partial(\boldsymbol{m}\cdot\boldsymbol{\Omega})/\partial J_2 = 0$ at the origin.
- Tangent singularity at $(J_2^*, 0)$ for the modes $\boldsymbol{m}$ satisfying $-1 < m_3/m_2 < -1/3$. For such a mode, the singular point J_2^* is given by the solution to the equation
$$\left.\frac{\partial}{\partial J_2}\right|_{J_3=0} \boldsymbol{m}\cdot\boldsymbol{\Omega} = 0, \tag{93}$$
which reads
$$-\frac{1}{2}\left(1+\frac{J_2}{\sqrt{J_2^2+4GMb}}\right)+\frac{2}{3}\frac{GMb}{J_2^2+4GMb} = \frac{m_3}{m_2}. \tag{94}$$
We remark that the left-hand-side of (94) is a decreasing function of J_2, and its range is $(-1,-1/3)$ for $J_2\in(0,\infty)$. Thus m_3/m_2 must be in the interval $(-1,-1/3)$. The origin, namely $J_2^*=0$, results in the special vertex singularity for the modes satisfying $m_2+3m_3=0$.
- Line singularity on J_3 axis for the modes $\boldsymbol{m}$ satisfying $m_2=-2m_3$.
- A singularity at infinity appears for any mode $\boldsymbol{m}$. Estimations of $\nu(\boldsymbol{J})$ and $\mu(\boldsymbol{J})$ are
$$\nu(\boldsymbol{J})\sim(J_2+J_3)^{-4},\quad \mu(\boldsymbol{J})\sim(J_2+J_3)^{-3}, \tag{95}$$
since $\Omega_2\sim\Omega_3\sim(J_2+J_3)^{-3}$, $f_0\sim\tilde{E}^{5/2}$, $\tilde{E}\sim(J_2+J_3)^{-2}$, and taking into account the J_2 factor for ν appearing in (92).

No critical singularity appears in the isochrone model. These singularities are arranged in Table 7 with asymptotic dampings and frequencies.

The leading dampings are t^{-3}, $t^{-1.5}$, t^{-2} and $t^{-2/3}$ for the vertex, tangent, line and infinity singularities respectively. We remark that the leading order of the function ν is $\nu\sim J_2$ around $J_2=0$ due to the J_2 factor of ν in (92), thus the leading damping rates

for the vertex and line singularities respectively are not t^{-2} and t^{-1}, but t^{-3} and t^{-2} . The dominant, i.e. slowest, decay is $t^{-2/3}$ with zero frequency.

In the next subsection we will observe the temporal evolution of the expected value of the observable $A(\boldsymbol{\theta}) = \sin(n_2\theta_2 + n_3\theta_2)$ with respect to the exact solution

$$f_1(\boldsymbol{\theta}, \boldsymbol{J}, t) = f_1(\boldsymbol{\theta} - \boldsymbol{\Omega}(\boldsymbol{J})t, \boldsymbol{J}, t = 0). \tag{96}$$

The mode (n_2, n_3) corresponds to the mode of perturbation (89). The expected value is:

$$\langle A \rangle_1 (t) = \int A(\boldsymbol{\theta}) f_1(\boldsymbol{\theta}, \boldsymbol{J}, t) d\boldsymbol{\theta} d\boldsymbol{J}. \tag{97}$$

For our interests, the prefactor of $\langle A \rangle_1 (t)$ is not crucial; therefore we redefine $\langle A \rangle_1 (t)$ as

$$\langle A \rangle_1 (t) = \int_0^\infty \int_0^\infty J_2 f_0(\boldsymbol{J}) \sin((n_2\Omega_2(\boldsymbol{J}) + n_3\Omega_3(\boldsymbol{J}))t) dJ_2 dJ_3 \tag{98}$$

in the following. For this sine observable, the leading vertex, tangent and infinity singularities survive, but the leading line singularity is expected to be cancelled looking at Table 2, since the corresponding exponents are $a_1 = 1$ and $a_2 = 0$. From the line singularity, therefore, the second leading damping t^{-3} should arise instead of the leading damping t^{-2}. However, since the line singularity is never dominant, this cancellation does not affect the following discussions.

7.4. Numerical check

We choose three modes: $(n_2, n_3) = (1, 1), (2, -1)$ and $(3, -2)$. The mode $(1, 1)$ has vertex and infinity singularities, $(2, -1)$ has all four singularities, and $(3, -2)$ has all four except the line singularity. To perform the numerical integration of (98), we set the parameters as $G = M = b = 1$. The exact solutions (98) are shown in figure 7.

The mode $(1, 1)$ shows $t^{-2/3}$ damping without oscillation as the theory predicted. This mode also has a vertex singularity, which gives a non-zero frequency, but no oscillation is observed in the asymptotic time region: the vertex singularity contribution is expected to damp as t^{-3}, which may be too fast to be visible at large times.

The modes $(2, -1)$ and $(3, -2)$ asymptotically damp as $t^{-2/3}$ as predicted, but they have oscillations. At variance with the mode $(1, 1)$, both these modes have a tangent singularity, which gives a rather slow damping $t^{-1.5}$ with non-zero frequency. To confirm that there is a contribution from the tangent singularity, we show the power spectra of $\langle A \rangle_1 (t)$ in figure 8. The peaks of the power spectra are in good agreement with the theoretically predicted frequency $|m_2\Omega_2(J_2^*, 0) + m_3\Omega_3(J_2^*, 0)|$, where J_2^* is the solution to (94).

As mentioned above, to study the true Vlasov equation, we should also estimate the $c_k(\boldsymbol{m}, \boldsymbol{J})$ functions, which depend on the biorthogonal functions $u_k(\boldsymbol{q})$.

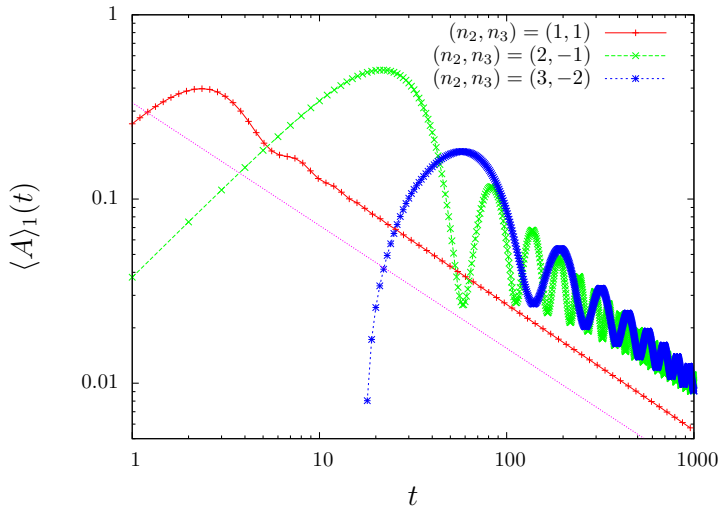

Figure 7. Damping in the isochrone model for the observable $A = \sin(n_2\theta_2 + n_3\theta_3)$. $(n_2, n_3) = (1, 1)$ (red plus), $(2, -1)$ (green cross) and $(3, -2)$ (blue star). The purple guide line is proportional to $t^{-2/3}$. $\langle A \rangle(t)$ is computed by using (98) with cutoff at $J_2 = J_3 = 20$.

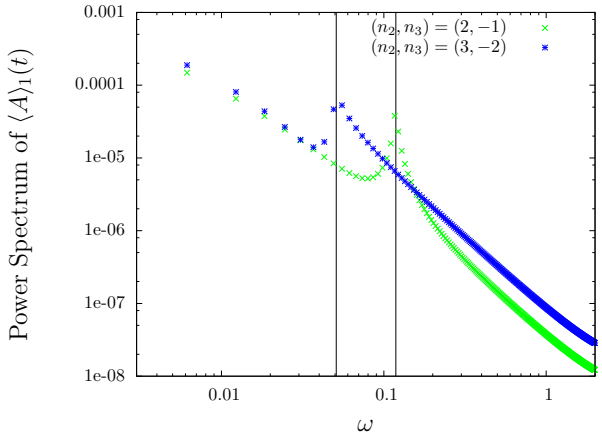

Figure 8. Power spectra of $\langle A \rangle_1(t)$ for the modes $(2, -1)$ (green cross points) and $(3, -2)$ (blue star points). The two vertical lines indicate $\omega = 0.1185$ and 0.0509, which are predicted theoretically for the modes $(2, -1)$ and $(3, -2)$ respectively as $|m_2\Omega_2(J_2^*, 0) + m_3\Omega_3(J_2^*, 0)|$ with J_2^* the solution to (94). The power spectra are computed from time series with time slice 1 in the time interval $[77, 1100]$ to avoid an early transient time region.

8. Conclusion

When a stable inhomogeneous stationary state of a Vlasov equation is perturbed, the asymptotic damping of the perturbation is algebraic, no matter how regular the stationary state and perturbation are. The damping rate and frequency are controlled by the singularities on the real axis of the Fourier-Laplace transform of the perturbation. In this paper, in systems with two spatial dimensions, we have classified

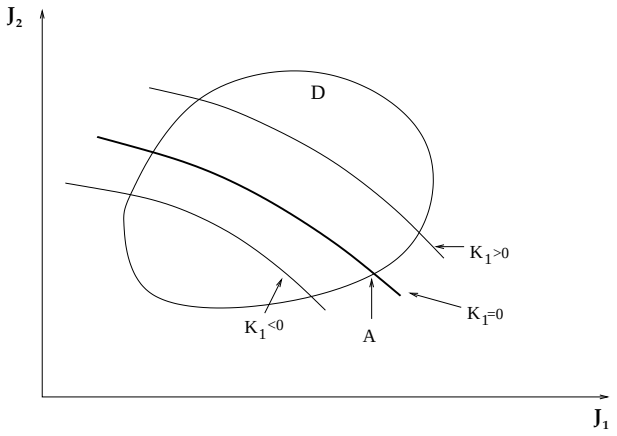

Figure A1. The boundary of D is regular close to point A, its intersection with the curve $\mu(J_1, J_2) = x_0$, that is $K_1 = 0$

.

these singularities into vertex, tangent, critical, line and infinity singularities, and have given damping rate and frequency in each case. This classification is also valid for three dimensional spherically symmetric stationary states, since they reduce to the two-dimensional case thanks to symmetry. The resulting picture is much richer than in one spatial dimension [22]. We have illustrated the theory on a toy model, and on an advection equation associated with the isochrone model, a simple model for self-gravitating systems: tests in these models show that the singularity analysis captures very well the observed damping.

The main goal of this theory is a better understanding of the asymptotic relaxation of self gravitating systems. To achieve this goal, a detailed study of the classical expansion of a perturbation on a biorthogonal basis should be coupled to the singularity analysis we have presented here.

Acknowledgments

The authors thank Magali Ribot for suggesting the power series expansions (E.16). This work is partially supported by the ANR-09-JCJC-009401 INTERLOP project. Y.Y.Y. acknowledges the support of a Grant-in-Aid for Scientific Research (C) 23560069.

Appendix A. Analytic continuation

The starting point is the following formula for $\varphi(z)$, valid for $\mathrm{Im}(z) > 0$:

$$\varphi(z) = \int_{D \subset \mathbb{R}^2} \frac{\nu(J_1, J_2)}{\mu(J_1, J_2) - z} \, .$$

We want to understand the regularity of $\varphi(z)$ close to $z = x_0 \in \mathbb{R}$.

Assuming that x_0 is not a critical value for the function μ (condition i), the equation $\mu(J_1, J_2) = x_0$ defines one or several curves on the (J_1, J_2) plane. We treat here the case

with one curve, the argument carries over easily to the case of several curves.

It is then possible to use a new set of variables K_1, K_2 fulfilling the two conditions:
a) $K_1 = \mu(J_1, J_2) - x_0$
b) K_2 is such that the Jacobian $dK_1 dK_2 / dJ_1 dJ_2$ never vanishes. We do not need to further specify K_2.

Then, with a suitable definition of $\tilde{\nu}$:

$$\varphi(z) = \int_{\tilde{D} \subset \mathbb{R}^2} \frac{\tilde{\nu}(K_1, K_2)}{K_1 - (z - x_0)} dK_1 dK_2 \ .$$

Integrating over K_2 first:

$$\varphi(z) = \int_{K_1^{(m)}}^{K_1^{(M)}} \frac{dK_1}{K_1 - (z - x_0)} \int_{K_2^{(m)}(K_1)}^{K_2^{(M)}(K_1)} \tilde{\nu}(K_1, K_2) dK_2 \ .$$

If the boundary of the domain D is regular around its intersection with the curve $K_1 = 0$ (condition ii) (see figure A1, point A), then $K_2^{(M)}(K_1)$ and $K_2^{(m)}(K_1)$ are regular functions of K_1, and we are left with the single integral

$$\varphi(z) = \int_{K_1^{(m)}}^{K_1^{(M)}} \frac{h(K_1)}{K_1 - (z - x_0)} dK_1$$

where h is a regular function. The usual Landau continuation argument then ensures that $\varphi(z)$ is regular at $z = x_0$, unless $K_1^{(m)} = 0$ or $K_1^{(M)} = 0$ (condition iii).

Thus, under conditions i), ii) and iii), $\varphi(z)$ is not singular at $z = x_0$. Breaking one of these conditions yields a critical (section 3.5), vertex (section 3.3) and tangent (section 3.4) singularity respectively.

Appendix B. Vertex singularity

Let us compute the leading singularity of

$$\varphi(z) = \int_U \frac{u^k v^l}{u - (z - x_0)} du dv. \tag{B.1}$$

The origin $(u, v) = (0, 0)$ is on the boundary of the domain U, and is a singular point. We assume that the boundary of the domain U is locally approximated by two lines around the origin, and that the line $u = 0$ does not coincide with one of such boundary lines. We can classify the shapes of the domain in three cases: (i) the two lines are in the $u > 0$ half plane; (ii) the two lines are in the $u < 0$ half plane; (iii) one line is in the $u > 0$ half plane, and the other in the $u < 0$ half plane. Case (ii) is made identical to case (i) by changing the sign of u, z and C if necessary. Thus we consider case (i) and case (iii). Remembering that the line $u = 0$ does not coincide with the boundary of U, we can further classify U into the following four types:

$$U_1 = \{(u, v) \mid 0 < u < \epsilon, \ \beta u < v < \alpha u\}. \tag{B.2}$$

$$\begin{aligned} U_2 = \{&(u, v) \mid 0 < u < \epsilon, \ \alpha u < v < \delta \text{ or } \delta < v < \beta u\} \\ &\cup \{(u, v) \mid -\epsilon < u < 0, \ -\delta < v < \delta\}. \end{aligned} \tag{B.3}$$

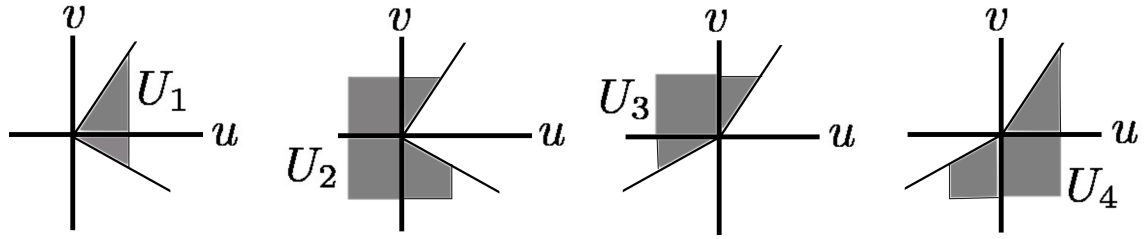

Figure B1. Four types of domain U for the vertex singularity.

$$U_3 = \{(u,v) \mid 0 < u < \epsilon,\ \alpha u < v < \delta\} \\ \cup \{(u,v) \mid -\epsilon < u < 0,\ \beta u < v < \delta\}. \tag{B.4}$$

$$U_4 = \{(u,v) \mid 0 < u < \epsilon,\ \delta < v < \alpha u\} \\ \cup \{(u,v) \mid -\epsilon < u < 0,\ \delta < v < \beta u\}. \tag{B.5}$$

The domains U_1 and U_2 correspond to case (i), and U_3 and U_4 to case (iii). δ, ϵ, α and β are constants. See figure B1 for schematic pictures of the domains. We first note that the integral over the domain

$$U_{\text{regular}} = \{(u,v) \mid -\epsilon < u < \epsilon,\ \alpha u < v < \delta\} \tag{B.6}$$

does not give any singularity for the function (B.1). This fact is immediately obtained by performing the integral over v:

$$\int_{-\epsilon}^{\epsilon} \frac{u^k du}{u-(z-x_0)} \int_{\alpha u}^{\delta} v^l dv = \int_{-\epsilon}^{\epsilon} \frac{u^k}{u-(z-x_0)} \frac{\delta^{l+1} - (\alpha u)^{l+1}}{l+1}\, du \tag{B.7}$$

and using Appendix E. Adding or subtracting such a regular domain, domains U_2, U_3 and U_4 can be reduced to U_1. Thus, what we have to consider are integrals of the form:

$$\varphi(z) = \int_0^{\epsilon} \frac{u^k du}{u-(z-x_0)} \int_{\beta u}^{\alpha u} v^l dv = \frac{\alpha^{l+1} - \beta^{l+1}}{l+1} \int_0^{\epsilon} \frac{u^{k+l+1}}{u-(z-x_0)} du \tag{B.8}$$

Using Appendix E again, the leading singularity of $\phi(x) = \lim_{y\to 0^+} \varphi(x+iy)$ at x_0 is

$$\phi_{x_0}^{\text{sing}}(x) = c_1 (x-x_0)^{k+l+1} \ln|x-x_0| + c_2 (x-x_0)^{k+l+1} H(x-x_0) \tag{B.9}$$

except in the non-generic situation $\beta = -\alpha$, l odd.

Appendix C. Tangent singularity

Changing variables to $u = J_1^2 + J_2, v = J_1$, the leading singular part of the function $\varphi(z)$ is:

$$\varphi(z) = C \int_0^{u_0} \frac{du}{u-(z-x_0)} \int_{-\sqrt{u}}^{\sqrt{u}} v^{a_1} (u-v^2)^{a_2} dv \tag{C.1}$$

$$= \sum_k c_k \int_0^{u_0} \frac{u^{a_2-k} du}{u-(z-x_0)} \int_{-\sqrt{u}}^{\sqrt{u}} v^{a_1+2k} dv. \tag{C.2}$$

The integral over v is computed as

$$\int_{-\sqrt{u}}^{\sqrt{u}} v^{a_1+2k} dv = \frac{1}{1+a_1+2k}(1-(-1)^{1+a_1+2k})u^{(1+a_1+2k)/2}.$$

Thus we have

$$\varphi(z) = \sum_k c_k \frac{1-(-1)^{1+a_1+2k}}{1+a_1+2k} \int_0^{u_0} \frac{u^{1/2+a_1/2+a_2}}{u-(z-x_0)} du.$$

The prefactor $1-(-1)^{1+a_1+2k} = 1-(-1)^{1+a_1}$ vanishes for any k when a_1 is odd, thus we may assume that a_1 is even. We are left with integrals as in (E.2), with $1/2+a_1/2+a_2 \notin \mathbb{Z}_+$. Thus the leading singularity is

$$\phi_{x_0}^{\rm sing}(x) = C_1(x-x_0)^{1/2+a_1/2+a_2} H(x-x_0) + C_2(x_0-x)^{1/2+a_1/2+a_2} H(x_0-x). \quad \text{(C.3)}$$

Appendix D. Critical singularity

Calling λ_1 and λ_2 the two eigenvalues of the Hessian of μ at the critical point, we expand $\mu(\boldsymbol{J})$ after an appropriate change of basis

$$\mu(\boldsymbol{J}) \simeq x_0 + \lambda_1(J_1-J_1^*)^2 + \lambda_2(J_2-J_2^*)^2. \quad \text{(D.1)}$$

We have to consider two cases: i) the critical point is a local extremum; ii) the critical point is a saddle.

Case i), $\lambda_1\lambda_2 > 0$: Without loss of generality, we assume $\lambda_1 > 0$, $\lambda_2 > 0$. Using the leading order approximation (34) for ν and performing the usual shifting and scaling of variables, we obtain the leading singular part of $\varphi(z)$ as

$$\varphi(z) = C \int_U \frac{J_1^{a_1} J_2^{a_2}}{J_1^2+J_2^2-(z-x_0)} dJ_1 dJ_2 \quad \text{(D.2)}$$

$$= C \int_0^{2\pi} \cos^{a_1}\alpha \sin^{a_2}\alpha d\alpha \int_0^{\varepsilon} \frac{r^{1+a_1+a_2}}{r^2-(z-x_0)} dr \quad \text{(D.3)}$$

where (r,α) are the polar coordinates on the (J_1,J_2) plane. A change of variable $u=r^2$ reduces the integral over r to the form (E.2) and we conclude that the leading singularity is

$$\phi^{\rm sing} = \begin{cases} C_1(x-x_0)^{(a_1+a_2)/2}\ln|x-x_0| & \\ \quad +C_2(x-x_0)^{(a_1+a_2)/2}H(x-x_0) & a_1,a_2 : \text{even} \\ 0 & \text{otherwise.} \end{cases} \quad \text{(D.4)}$$

Case ii), $\lambda_1\lambda_2 < 0$:

Without loss of generality, we may assume, shifting and scaling J_1 and J_2, that $\lambda_1 = 1$, $\lambda_2 = -1$, and the saddle is at $(J_1,J_2)=(0,0)$. We need then to study

$$\varphi(z) = \int_{-c_1}^{c_1}\int_{-c_2}^{c_2} \frac{J_1^{a_1}J_2^{a_2}}{J_1^2-J_2^2-(z-x_0)} dJ_1 dJ_2. \quad \text{(D.5)}$$

The function $\varphi(z)$ is zero except for even a_1 and a_2. We perform the change of variables

$$j_1 = J_1 + J_2 \ , \ j_2 = J_1 - J_2 \ ; \ dj_1\, dj_2 = 2\, dJ_1\, dJ_2. \tag{D.6}$$

Forgetting a constant factor and modifying the integration domain (the important thing is to integrate over a neighborhood of $(0,0)$), we are led to study

$$\begin{aligned}\varphi(z) &= \int_{-c_1}^{c_1}\int_{-c_2}^{c_2} \frac{(j_1+j_2)^{a_1}(j_1-j_2)^{a_2}}{j_1 j_2 - (z-x_0)} dj_1 dj_2 \\ &= \sum_{k=0}^{a_1}\sum_{l=0}^{a_2} C_{kl} \int_{-c_1}^{c_1}\int_{-c_2}^{c_2} \frac{j_1^{k+l} j_2^{a_1+a_2-k-l}}{j_1 j_2 - (z-x_0)} dj_1 dj_2.\end{aligned} \tag{D.7}$$

After a further change of variables

$$u = j_1 j_2 \ , \ v = j_2 \ ; \ dj_1\, dj_2 = \frac{1}{|v|} du\, dv \tag{D.8}$$

we obtain

$$\begin{aligned}\varphi(z) = &\sum_{k=0}^{a_1}\sum_{l=0}^{a_2} 2C_{kl} \\ &\times \left(\int_0^{c_1 c_2} du \int_{u/c_1}^{c_2} dv + \int_{-c_1 c_2}^{0} du \int_{-u/c_1}^{c_2} dv \right) \frac{u^{k+l} v^{a_1+a_2-2(k+l)}}{(u-(z-x_0))|v|}.\end{aligned} \tag{D.9}$$

Remembering that $a_1 + a_2$ is even, we perform the integration over v:

$$\begin{aligned}\varphi(z) = &\sum_{k=0}^{a_1}\sum_{l=0}^{a_2} 2C_{kl} \int_{-c_1 c_2}^{c_1 c_2} \frac{u^{k+l}}{(u-(z-x_0))} du \\ &\times \begin{cases} \frac{1}{\gamma}(c_2^\gamma - (u/c_1)^\gamma), & \gamma = a_1 + a_2 - 2(k+l) \neq 0 \\ \ln|c_2| - \ln|u/c_1|, & \gamma = a_1 + a_2 - 2(k+l) = 0. \end{cases}\end{aligned} \tag{D.10}$$

The terms with $2(k+l) \neq a_1 + a_2$ are not singular, so we are left with

$$\sum_{k+l=(a_1+a_2)/2} C_{kl} \int_{-c}^{c} \frac{u^{k+l} \ln|u|}{u-z} du. \tag{D.11}$$

According to Appendix E again, the singularity of $\phi(x)$ is then

$$\phi^{\text{sing}}(x) = C_1 (x-x_0)^{(a_1+a_2)/2} \ln|x-x_0| + C_2 (x-x_0)^{(a_1+a_2)/2} H(x-x_0) \tag{D.12}$$

for a_1 and a_2 even.

Appendix E. Singularity computation

We first show that the function

$$\phi(x) = \lim_{y\to 0^+} \int_{-c}^{c} \frac{u^\alpha}{u-(x+iy)} du, \quad \alpha \in \mathbb{Z}_+ \tag{E.1}$$

does not have any singularity. Then we compute singularities of the functions

$$\phi(x) = \lim_{y\to 0^+} \int_{0}^{c} \frac{u^\alpha}{u-(x+iy)} du, \quad \alpha \in \mathbb{R} \setminus \{\cdots, -3, -2, -1\}, \tag{E.2}$$

and

$$\phi(x) = \lim_{y\to 0^+} \int_{-c}^{c} \frac{u^\alpha \ln|u|}{u-(x+iy)} du, \quad \alpha \in \mathbb{Z}_+. \tag{E.3}$$

The constant c is assumed to be positive in the above three functions. All the singularities found in this paper reduce to a computation of the singularity close to $x = 0$ of one of the above two functions, (E.2) and (E.3). We show in this appendix that singular parts of ϕ are

$$\phi^{\text{sing}}(x) = -x^\alpha \ln|x| + i\pi x^\alpha H(x), \quad \alpha \in \mathbb{Z}_+ \tag{E.4}$$

and

$$\phi^{\text{sing}}(x) = C_1 x^\alpha H(x) + C_2(-x)^\alpha H(-x) + i\pi x^\alpha H(x), \quad \alpha \in \mathbb{R}\setminus\mathbb{Z} \tag{E.5}$$

for the function (E.2), and

$$\phi^{\text{sing}}(x) = C x^\alpha H(x) + i\pi x^\alpha \ln|x|, \quad \alpha \in \mathbb{Z}_+ \tag{E.6}$$

for the function (E.3).

Appendix E.1. No singularity of the function (E.1)

We start from the function (E.1)

$$\phi(x) = \lim_{y\to 0+} \left[\int_{-c}^{c} \frac{(u-x)u^\alpha}{(u-x)^2+y^2} du + iy \int_{-c}^{c} \frac{u^\alpha}{(u-x)^2+y^2} du \right]. \tag{E.7}$$

We denote the real and the imaginary parts of $\phi(x)$ by $\phi_R(x)$ and $\phi_I(x)$ respectively. The imaginary part $\phi_I(x)$ can be computed using the change of variable $s = (u-x)/y$:

$$\phi_I(x) = \pi x^\alpha (H(x+c) - H(x-c)), \tag{E.8}$$

where H is the Heaviside step function. Thus $\phi_I(x)$ has no singularity around $x = 0$.

The real part is simply:

$$\begin{aligned} \phi_R(x) &= PV \int_{-c}^{c} \frac{u^\alpha}{u-x} du \\ &= PV \int_{-c}^{c} \frac{x^\alpha}{u-x} du + \sum_{l=0}^{\alpha-1} C_{l,\alpha} x^l \int_{-c}^{c} (u-x)^{\alpha-l-1} du \end{aligned} \tag{E.9}$$

where PV denotes the principal value. The sum on the right-hand-side is clearly regular, and the first term gives:

$$PV \int_{-c}^{c} \frac{x^\alpha}{u-x} du = x^\alpha (\ln|c-x| - \ln|-c-x|), \tag{E.10}$$

so that no singularity appears around $x = 0$.

Appendix E.2. Singularity of the function (E.2)

We study the function (E.2), which differs from the function (E.1) in the lower bound of the integral. The imaginary part, ϕ_I, is then:

$$\phi_I(x) = \pi x^\alpha (H(x) - H(x-c)), \tag{E.11}$$

and hence the singularity of ϕ_I around $x = 0$ is

$$\phi_I^{\text{sing}}(x) = \pi x^\alpha H(x). \tag{E.12}$$

The real part is also directly obtained using equation (E.10):

$$\phi_R(x) = x^\alpha (\ln|c-x| - \ln|-x|) \tag{E.13}$$

for $\alpha \in \mathbb{Z}_+$. Thus, the singularity of ϕ_R around $x = 0$ is

$$\phi_R^{\text{sing}}(x) = -x^\alpha \ln|x|, \quad \alpha \in \mathbb{Z}_+. \tag{E.14}$$

Combining real and imaginary part gives (E.4).

The final step for the function (E.2) is to investigate the real part for $\alpha \in \mathbb{R} \setminus \mathbb{Z}$. We divide $\phi_R(x)$ in two parts:

$$\phi_R(x) = \lim_{\epsilon \to 0} \left(\int_0^{|x|-\epsilon} \frac{u^\alpha}{u-x} du + \int_{|x|+\epsilon}^{c} \frac{u^\alpha}{u-x} du \right). \tag{E.15}$$

This division is just the definition of the principal value for $x > 0$, and is also valid for $x < 0$. We then use the expansions, for $u < |x|$ and $u > |x|$ respectively:

$$\frac{1}{u-x} = \frac{-1}{x} \sum_{k=0}^{\infty} \left(\frac{u}{x}\right)^k \quad ; \quad \frac{1}{u-x} = \frac{1}{u} \sum_{k=0}^{\infty} \left(\frac{x}{u}\right)^k. \tag{E.16}$$

Substituting the above expressions into (E.15) and remembering $\alpha \in \mathbb{R} \setminus \mathbb{Z}$, we have

$$\phi_R(x) = \begin{cases} -x^\alpha \sum_{k=0}^{\infty} \left(\frac{1}{\alpha+k+1} + \frac{1}{\alpha-k}\right) + \sum_{k=0}^{\infty} x^k \frac{c^{\alpha-k}}{\alpha-k} & x > 0, \\ (-x)^\alpha \sum_{k=0}^{\infty} \left(\frac{(-1)^k}{\alpha+k+1} + \frac{(-1)^{k+1}}{\alpha-k}\right) + \sum_{k=0}^{\infty} x^k \frac{c^{\alpha-k}}{\alpha-k} & x < 0. \end{cases} \tag{E.17}$$

Note that all series converge. The second series for $x > 0$ and $x < 0$ exactly coincide, hence they do not contribute any singularity. The singularity comes from the first series and is:

$$\phi_R^{\text{sing}}(x) = C_1 x^\alpha H(x) + C_2 (-x)^\alpha H(-x), \quad \alpha \in \mathbb{R} \setminus \mathbb{Z}. \tag{E.18}$$

Consequently, we have proved (E.5) for the function (E.2).

Appendix E.3. Singularity of the function (E.3)

The imaginary part of the function (E.3), denoted by $\phi_I(x)$, is

$$\phi_I(x) = \pi x^\alpha \ln|x| (H(x+c) - H(x-c)), \tag{E.19}$$

and the singularity around $x = 0$ is

$$\phi_I^{\text{sing}}(x) = \pi x^\alpha \ln|x|. \tag{E.20}$$

To compute the real part, we rewrite the integrand as done in (E.9):

$$\phi_R(x) = PV \int_{-c}^{c} \left[\frac{x^\alpha}{u-x} + \sum_{l=0}^{\alpha-1} {}_\alpha C_l (u-x)^{\alpha-l-1} x^k \right] \ln|u| du. \tag{E.21}$$

We remark that the integral

$$\int_{-c}^{c} u^n \ln|u| du \quad (n \in \mathbb{Z}_+) \tag{E.22}$$

can be performed in the sense of improper integral, and converges to a finite value. Thus, concentrating on the singularity, the real part is reduced to

$$\begin{aligned} \phi_R(x) &= x^\alpha \; PV \int_{-c}^{c} \frac{\ln|u|}{u-x} du \\ &= x^\alpha \lim_{\epsilon \to 0} \left(\int_{-|x|+\epsilon}^{|x|-\epsilon} + \int_{-c}^{-|x|-\epsilon} + \int_{|x|+\epsilon}^{c} \right) \frac{\ln|u|}{u-x} du. \end{aligned} \tag{E.23}$$

Using expansion (E.16), we obtain

$$\int_{-|x|+\epsilon}^{|x|-\epsilon} \frac{\ln|u|}{u-x} du = \sum_{k=0}^{\infty} \frac{-2}{x^{2k+1}} \left[\frac{(|x|-\epsilon)^{2k+1}}{2k+1} \ln||x|-\epsilon| - \frac{(|x|-\epsilon)^{2k+1}}{(2k+1)^2} \right] \tag{E.24}$$

and

$$\begin{aligned} &\left(\int_{-c}^{-|x|-\epsilon} + \int_{|x|+\epsilon}^{c} \right) \frac{\ln|u|}{u-x} du \\ &\simeq \sum_{k=0}^{\infty} 2x^{2k+1} \left(\frac{(|x|+\epsilon)^{-(2k+1)}}{2k+1} \ln||x|+\epsilon| + \frac{(|x|+\epsilon)^{-(2k+1)}}{(2k+1)^2} \right), \end{aligned} \tag{E.25}$$

where we have omitted regular functions in (E.25). The logarithmic terms are cancelled by adding (E.24) and (E.25) and taking the limit $\epsilon \to 0$; hence the singularity of $\phi_R(x)$ is:

$$\phi_R^{\text{sing}}(x) = C x^\alpha H(x). \tag{E.26}$$

The imaginary part (E.20) and the real part (E.26) prove (E.6) for the function (E.3).

Appendix E.4. Relative sign between modes $\boldsymbol{m}$ and $-\boldsymbol{m}$

Coming back to the functions F's and G's, we are interested in singularities of the function

$$\varphi(z; \boldsymbol{m}) = \int \frac{\nu(\boldsymbol{J})}{\boldsymbol{m} \cdot \boldsymbol{\Omega}(\boldsymbol{J}) - z} d\boldsymbol{J}. \tag{E.27}$$

To discuss a possible cancellation between the modes $\boldsymbol{m}$ and $-\boldsymbol{m}$, we show a relation between the above function and

$$\varphi(z; -\boldsymbol{m}) = \int \frac{\nu(\boldsymbol{J})}{-\boldsymbol{m} \cdot \boldsymbol{\Omega}(\boldsymbol{J}) - z} d\boldsymbol{J}. \tag{E.28}$$

We note that the numerator $\nu(\boldsymbol{J})$ may also depend on $\boldsymbol{m}$; in this case one would have to discuss the sign of the numerator separately; we ignore this dependence in this section.

Remembering that the singularity of the function (E.27) results in one of the two types of functions (E.2) and (E.3), we consider the relation between

$$\phi^+_{x_0}(x) = \lim_{y\to 0+} \int \frac{h(u)}{u-(x-x_0)-iy} du \tag{E.29}$$

and

$$\phi^-_{-x_0}(x) = -\lim_{y\to 0+} \int \frac{h(u)}{u+(x+x_0)+iy} du \tag{E.30}$$

where $h(u)$ is u^α ($\alpha \in \mathbb{Z}_+ \cup (\mathbb{R}\setminus\mathbb{Z})$ or $u^\alpha \ln|u|$ ($\alpha \in \mathbb{Z}_+$), and $x_0 = \boldsymbol{m}\cdot\boldsymbol{\Omega}(\boldsymbol{J}^*) \in \mathbb{R}$ with a special point $\boldsymbol{J} = \boldsymbol{J}^*$. $\phi^-_{-x_0}$ is obtained by changing the signs of the prefactor, x and y in $\phi^+_{x_0}$, thus the singular points of $\phi^+_{x_0}(x)$ and $\phi^-_{-x_0}(x)$ are x_0 and $-x_0$ respectively. If $x_0 \neq 0$, no cancellation occurs in general due to the different singular points. If $x_0 = 0$, a cancellation may occur depending on the relative sign of the singularities for the modes $\boldsymbol{m}$ and $-\boldsymbol{m}$. The change of sign of y implies the change of sign of the imaginary part, and we use $H(-x) = 1 - H(x)$. Hence the relation between the singularities of $\phi^+_0(x)$ and $\phi^-_0(x)$ is:

$$\phi^{-,\mathrm{sing}}_0(x) = (-1)^{1+\alpha}\phi^{+,\mathrm{sing}}_0(x), \quad \alpha \in \mathbb{Z}_+ \tag{E.31}$$

for the singularity (E.4), and

$$\phi^{-,\mathrm{sing}}_0(x) = (-1)^{\alpha}\phi^{+,\mathrm{sing}}_0(x), \quad \alpha \in \mathbb{Z}_+ \tag{E.32}$$

for the singularity (E.6). The relations (E.31) and (E.32) imply that, for instance, singularities of $\varphi(z;\boldsymbol{m}) + \varphi(z;-\boldsymbol{m})$ and of $\varphi(z;\boldsymbol{m}) - \varphi(z;-\boldsymbol{m})$ cancel respectively if α is 0 or positive even and $x_0 = 0$. There is no simple relation such as (E.31) for singularity (E.5), thus no cancellation is expected in general.

[1] Landau L 1946, *J. Phys. USSR* **10** 25
[2] Maslov V P and Fedoryuk M V 1985 *Mat. Sb. (N.S.)* **127(169)** 445
[3] Degond P 1986 *Trans. Am. Math. Soc.* **294** 435
[4] Weitzner H 1967 *Magneto-Fluid and Plasma Dynamics* edited by Grad H (American Mathematical Society, Providence R.I.), and references therein
[5] Glassey R and Schaeffer J 1995 *Commun. Partial Differ. Equ.* **20** 647
[6] Mouhot C and Villani C 2011 *Acta Mathematica* **207** 29
[7] Mouhot C and Villani C 2010 *J. Math. Phys.* **51** 015204
[8] Lin S and Zeng C 2011 *Comm. Math. Phys.* **306** 291
[9] Kalnajs A J 1977 *Astrophysical J.* **212** 637
[10] Polyachenko V L and Shukhman I G 1981 *Soviet Astronomy (Tr. Astr. Zhurn.)* **25** 533
[11] Binney J and Tremaine S 2008 *Galactic Dynamics Second Edition* (Princeton University Press)
[12] Jain K, Bouchet F and Mukamel D 2007 *J. Stat. Mech.* P11008
[13] Campa A and Chavanis P H 2010 *J. Stat. Mech.* P06001
[14] Bachelard R et al. 2011 *J. Stat. Mech.* P03022
[15] Mathur S 1990 *Mon. Not. R. Astron. Soc.* **243** 529
[16] Weinberg M D 1994 *Astrophysical J.* **421** 481
[17] Vesperini E and Weinberg M D 2000 *Astrophysical J.* **534** 598
[18] Barré J, Olivetti A and Yamaguchi Y Y 2010 *J. Stat. Mech.* P08002
[19] Strogatz S H, Mirollo R E and Matthews P C 1992 *Phys. Rev. Lett.* **68** 2730
[20] Smereka P 1998 *Physica D* **124**,104

[21] Case K M 1960 *Phys. Fluids* **3** 143
[22] Barré J, Olivetti A and Yamaguchi Y 2011 *J. Phys. A* **44** 405502
[23] Clutton-Brock M 1972 *Astrophysics and Space Science* **16** 101
[24] Lighthill M J 1958 *Introduction to Fourier Analysis and Generalized Functions* (Cambridge University Press)